



---

# Single photons and coherent light in polarized quantum dot cavity QED

---

THESIS

submitted in partial fulfillment of the  
requirements for the degree of

MASTER OF SCIENCE

in

PHYSICS

Author :	David Nicolaas Leendert Kok
Student ID :	1055283
Group :	Dirk Bouwmeester
Supervisor :	Henk Snijders Wolfgang Löffler
2 <sup>nd</sup> corrector :	Carlo Beenakker

Leiden, The Netherlands, August 28, 2017



# Single photons and coherent light in polarized quantum dot cavity QED

**David Nicolaas Leendert Kok**

Huygens-Kamerlingh Onnes Laboratory, Leiden University  
P.O. Box 9500, 2300 RA Leiden, The Netherlands

August 28, 2017

## **Abstract**

High-fidelity single photon sources are required for quantum information technologies and fundamental research. Recently near-unity single photon purity and near-unity indistinguishability have been shown in resonantly pumped quantum dots embedded in an optical cavity. In this thesis we provide a theoretical framework and experimental results on polarization non-degenerate self-assembled InAs/GaAs quantum dots inside a polarization non-degenerate cavity, and show that by filtering the polarization the brightness of the single photon source can be enhanced. We furthermore describe the resulting output light analytically as a mixture of single photons and coherent light and derive a simple expression for the purity of the single photon source. Lastly we present pulsed measurements of this quantum dot-cavity system, and show that the purity of the single photon source is 98%.



# Acknowledgements

I wish to deeply thank Wolfgang Löffler and Henk Snijders for their supervision throughout this entire research project. This work would not have been possible without their guidance. Furthermore I thank John Frey and Justin Norman for their work on the development and fabrication of the samples.

A special thanks goes out to Marnix van de Stolpe with whom I collaborated on this project. Thank you for your insights during our daily discussions and the joint work on the simulations and measurements that led to the understanding of the semiclassical model.

Lastly I would like to thank my family for all their support throughout the year.



# Contents

<b>1</b>	<b>Introduction</b>	<b>1</b>
<b>2</b>	<b>Quantum dot CQED</b>	<b>3</b>
2.1	Continuous wave setup	3
2.1.1	Experimental setup	3
2.1.2	Materials	4
2.2	Theory	6
2.2.1	Derivation of the semiclassical model	6
2.2.2	Interpreting the transmission matrix	9
<b>3</b>	<b><math>g^2(0)</math> of mixed sources of light</b>	<b>13</b>
3.1	Quantum optical description of $g^2(0)$	13
3.2	Classical $g^2(0)$	18
3.3	Comparison between the two	20
<b>4</b>	<b>Combining theory and experiment</b>	<b>21</b>
4.1	Leaked laser light	21
4.2	Detector response	22
4.3	Simulations and measurements	23
4.3.1	Theoretical predictions	23
4.3.2	Comparison with measurement	23
<b>5</b>	<b>Rabi oscillations</b>	<b>27</b>
5.1	Theory of Rabi oscillations	27
5.2	Experimental design	30
5.3	Methods	31
5.3.1	$g^2(\tau)$ of a pumped system	32
5.4	Measurements	33
5.4.1	$g^2(\tau)$ of a pulsed quantum dot	33
5.4.2	Rabi oscillation measurements	35
5.4.3	Decay rate	37
<b>6</b>	<b>Conclusion</b>	<b>41</b>



# Introduction

A good understanding of the physics of light has brought about several revolutionary leaps of progress over the past centuries, ranging from the discovery of quantum mechanics to laser technology and all telecom applications. Technological developments in nano-scale material science over the past 20 years have allowed physicists to explore a new regime of optics, reaching low energy scales where photons, individual light particles, can reliably be created and studied.

These single photons have applications in fundamental optics research as well as in quantum encryption and key distribution [1] and quantum cluster computing [2]. For all these purposes it is important to have access to a high quality single photon source (SPS) – a device that can produce a single photon on demand. Although in practice no perfect SPS exists, a wide range of systems has been studied for their ability to produce single photons on demand [3–8] and some of these systems are approaching the limits required for practical applications.

The quality of a single photon source is quantified by three measures: brightness, purity and indistinguishability. The indistinguishability measures to what degree the produced photons are equal along all quantum mechanical degrees of freedom, i.e. to which degree these photons can be used for interference experiments. The purity describes the probability that only a single photon is emitted at a time, i.e. the absence of higher photon states. Lastly the brightness is given as the percentage of the time that triggering the SPS produces output light, as opposed to not emitting any light into the output mode.

Modern research on potential methods of creating a single photon source has shown highly promising SPS characteristics for samples consisting of a quantum dot (QD) excited on-resonance in an optical cavity [3, 8–18], presenting SPS's with indistinguishability and purities exceeding 97% and a brightness on the order of 50%. Our samples are also of this type, consisting of InAs/GaAs self-assembled quantum dots inside a micropillar cavity.

This thesis presents novel theoretical and experimental results to better understand and classify the behaviour of the quantum dots in our optical cavity and their properties as single

photon sources. We will first describe the experimental setup and the relevant theory for interpreting the measurement methods. The next section derives theoretical conditions that must be met when optimizing the QD-cavity system as a SPS. We will then proceed to explain how the SPS purity can be extracted from our measurements using a new theoretical approach, and use this result to conclude that the semiclassical model is in good agreement with measurements of the QD excited with a continuous wave laser. The final section of the thesis presents theory and experiment of the same sample excited with a pulsed laser, and interprets and discusses the results.

## Quantum dot CQED

In this section we will first explain the experimental setup and then explain the model of our quantum dot in an optical cavity. Although the model presented is semiclassical, we will refer to the cavity quantum electrodynamical theory at all points where the semiclassical model fails to describe phenomena of interest.

### 2.1 Continuous wave setup

Below we will introduce and discuss the experimental setup. The reason for discussing the setup before the theory is that this will shed light on the applicability of approximations made in the upcoming sections. We will study and discuss a single photon source consisting of a quantum dot in a cavity excited by a continuous wave laser tuned on resonance.

#### 2.1.1 Experimental setup

Figure 2.1 below shows a schematic overview of the setup.

The Fabry-Pérot cavity allows us to accurately measure the wavelength of the laser, which can be tuned between 930-945nm. The light from the laser is then sent to a quantum dot inside an optical cavity in the cold finger cryostat. The light transmitted through this cryostat is then, after passing through an output polariser, detected in a Hanbury-Brown-Twiss detector, for which we explain the motivation below.

As mentioned in the introduction one of the measures of the quality of a single photon source is its purity, which is the percentage of emitted light that consists of single photons. While a theoretical single photon source would have a purity of 100%, in practice purities of modern SPS's are as high as 97% [8]. It is therefore important to measure this purity, which can be done with a Hanbury-Brown-Twiss setup.

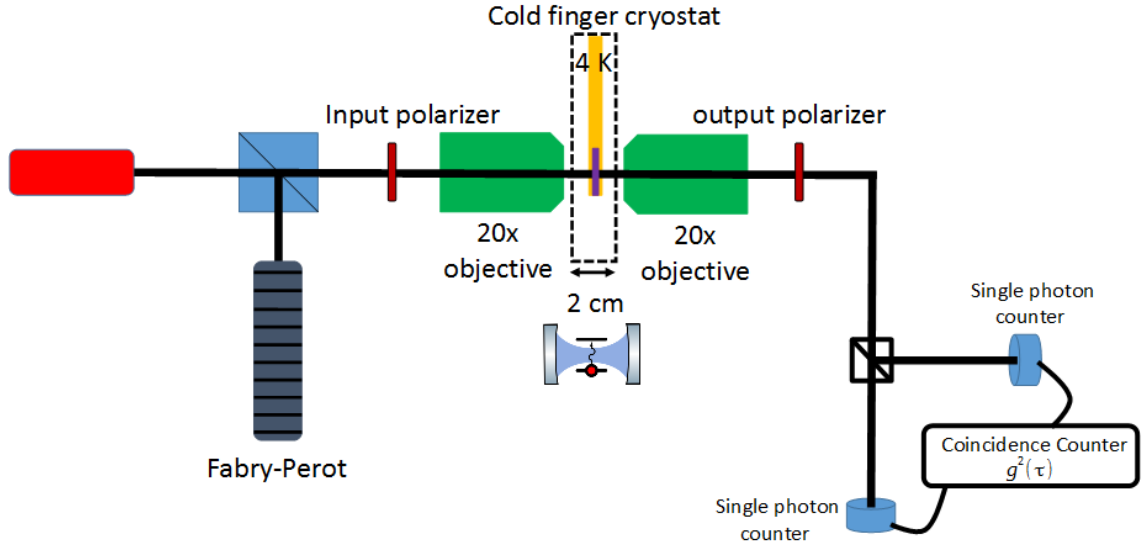


**Figure 2.1:** Schematic overview of the SPS consisting of a QD excited by an on-resonance continuous wave laser. The red box is the input laser, the sample is depicted by the purple bar inside the cold finger cryostat.

The Hanbury-Brown-Twiss setup consists of a 50/50 beamsplitter with each arm connected to a single photon detector. The signals from the single photon detectors are then led to a start-stop circuit board – one of the two detectors starts a timer on the circuit board, the other stops it and sends the measured time to the computer, thus producing a single coincidence count. Accumulating such coincidence counts over time in a histogram gives us the second-order autocorrelation function, i.e. the intensity autocorrelation function, of the light in the detection path. By ensuring that the optical path (in practice electrical path of the signal, but these are equivalent for our purposes) to the ‘stop’ single photon detector is longer than the path to the ‘start’ single photon detector we can even measure the autocorrelation function,  $g^2(\tau)$ , for (slightly) negative values of  $\tau$ .

From this autocorrelation function we can derive the purity of the SPS. A pure SPS emits only single photons, which means that it is impossible to detect a single photon on both detectors in this setup at the same time, i.e.  $g^2(0) = 0$  (see also figure 2.2). Any other light source will produce a non-zero amount of coincidences at zero time delay. Since for large values of  $\tau$  the autocorrelation function converges to some non-zero asymptote (which is conventionally normalised to 1) this means that the dip around  $\tau = 0$  allows us to deduce the purity of a SPS.

## 2.1.2 Materials

The quantum dot consists of an island of InAs embedded in single-crystalline GaAs, grown by the Stranski-Krastanov growth method, where the lattice mismatch between these two materials causes strain in the InAs which is released by island formation. The quantum dot forms a potential well for electrons and holes, thereby leading to quantized states, which is why

## $g^2(\tau)$ of a perfect single photon source

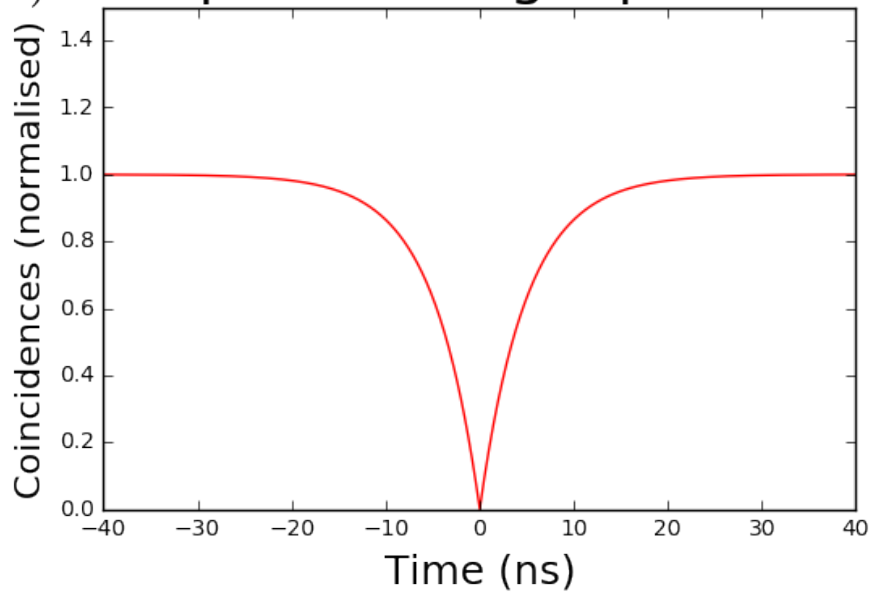


**Figure 2.2:** The second-order autocorrelation function of a perfect SPS.

a quantum dot is also called an artificial atom. A resonant laser can excite such an electron-hole pair (exciton), which can recombine and emit a single photon. During the production process of the layered optical cavity many such QDs are grown on a specific layer which will by the end of the fabrication process be in the middle of the sample, with layered Bragg reflectors forming thin film mirrors on both sides to produce a Fabry-Pérot cavity (see figure 2.3). A PIN junction enables us control over the resonance frequencies of the quantum dots inside through the quantum-confined Stark effect. We use this to tune an individual QD into resonance with the cavity. Important to note is that this mechanism only allows us to apply a global electric field, and does not allow fine-tuning of the local electrical configuration around a chosen QD.

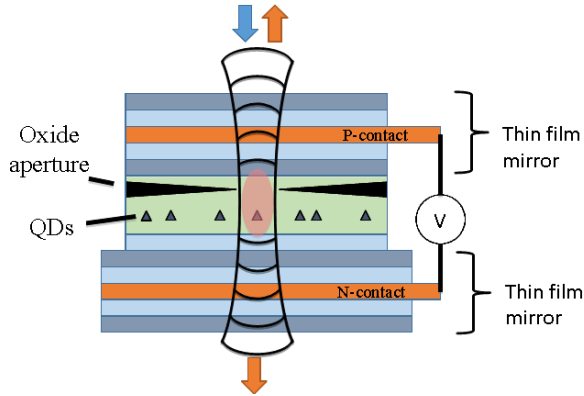


**Figure 2.3:** A schematic overview of the optical cavity and the quantum dots inside it.

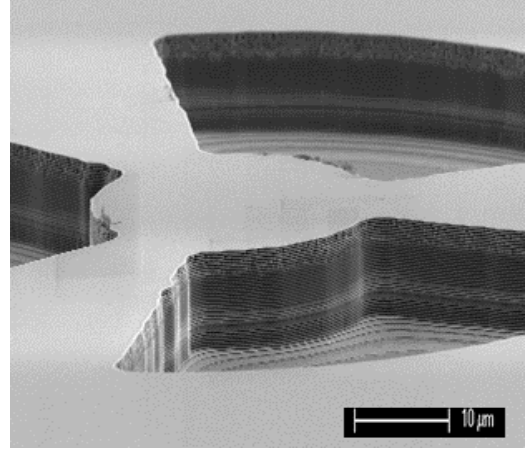


**Figure 2.4:** A scanning electron micrograph image of the cavity (center). Visible are the three trenches etched away from the layered structure, which allows for wet-chemical oxidation of an AlAs layer. This results in an intra-cavity aperture for in-plane confinement of the optical modes in the cavity.

The modes in the mirror are confined transversally by oxide apertures, created by etching away trenches around the desired location of the cavity and then oxidizing the sample (figure 2.4) [19].

## 2.2 Theory

In this section we will explain in detail the semiclassical model for a polarization non-degenerate quantum dot in a polarization non-degenerate optical cavity. We will explore the theoretical requirements for using this system as a good single photon source in terms of both the lab-tunable and fixed system parameters, and conclude that for maximum brightness of the SPS it is necessary that the optical cavity is polarization non-degenerate. In our analysis special attention will be paid to the parameter of quantum dot angle and its influence on the quality of the SPS.

### 2.2.1 Derivation of the semiclassical model

We are interested in modelling the transmission of light through a Fabry-Pérot cavity with a near-resonance quantum dot in it. There are multiple sources [20–22] for the amplitude transmission coefficient for single mode systems of this form, for example [22] giving the formula

$$t = \eta_{out} \frac{1}{1 - i\Delta + \frac{2C}{1 - i\Delta'}}.$$

Here  $\Delta$  is the detuning between the laser frequency and the cavity resonance frequency,  $\Delta'$  is the detuning between the laser and the QD resonance and  $C$  is the quantum dot-cavity coop-

erativity, which describes the interaction strength between light in the cavity and the quantum dot. We can interpret this formula as describing the Fabry-Pérot cavity as a Lorentzian lineshape filter and the quantum dot as a Lorentzian emitter inside the cavity.

The quantum dot in our system has two different excitation modes which emit orthogonally polarized light. Since the quantum dot is not perfectly circularly symmetrical these two modes also differ slightly in energy. This means that the formula above is not sufficient to describe the interaction of light with the quantum dot in our system. We therefore need a model that allows for two different quantum dot energies.

On top of this our cavity also has two orthogonal polarization modes, and since the cavity is also not perfectly circularly symmetrical (i.e. it is polarization non-degenerate) these two modes have different resonance frequencies. Together this means that in general we should in general introduce 4 coupling efficiencies. However due to the orthogonality and completeness of these sets of modes it is sufficient to introduce two parameters: the quantum dot-cavity cooperativity  $C$  as before and the angle  $\theta_{\text{QD}}$  between the quantum dot polarization basis and the cavity polarization basis. We need to be careful in defining  $\theta_{\text{QD}}$ , since there are many possible angles that can classify the interaction strength between the QD and the cavity. To introduce this angle we first say by convention that we will call the lowest energy cavity mode ‘Horizontal’ or H and the highest energy cavity mode ‘Vertical’ or V. We will call the lowest energy quantum dot mode X and the highest energy quantum dot mode Y, and we now define  $\theta_{\text{QD}}$  as the angle between the X mode and the H mode, see figure 2.5.

Next we adopt the notation introduced in [22]. For a given frequency of light we introduce the detuning with the horizontal polarization mode per round trip,  $\Delta_H$ . This is the phase picked up by light of input (angular) frequency  $\omega_{\text{laser}}$  in the cavity mode with horizontal polarization. We assume  $\Delta_H$  to be small compared to  $2\pi$ . Similarly we introduce the detuning with the vertical mode  $\Delta_V$ .

In a single mode system without a quantum dot the light would pick up a phase  $\exp(i\Delta_H) \approx 1 + i\Delta_H$  each round trip, so that the total amplitude transmission of the cavity would be  $1 + i\Delta_H + (i\Delta_H)^2 + (i\Delta_H)^3 + \dots = \frac{1}{1 - i\Delta_H}$ . Adding a quantum dot to the cavity with coupling strength  $2C$  and detuning  $\Delta'$  means that the amplitude change after a round trip becomes  $1 + \left(i\Delta_H + \frac{2C}{1 - i\Delta'}\right)$ , as the quantum dot has a Lorentzian lineshape (since the QD emission is limited by its exponential decay, so its frequency response function is the Fourier transform of a single exponential, corresponding to a Lorentzian). Summing over all round trips now gives the amplitude transmission formula from [22], i.e.

$$1 + \left(i\Delta_H + \frac{2C}{1 - i\Delta'}\right) + \left(i\Delta_H + \frac{2C}{1 - i\Delta'}\right)^2 + \dots = \frac{1}{1 - i\Delta_H + \frac{2C}{1 - i\Delta'}}.$$

We will now repeat this procedure of finding the amplitude change per round trip and then summing over infinitely many round trips in the polarization non-degenerate case. Note that now our amplitude is described by the 2-component Jones vector. To simplify notation we will work in the cavity frame of reference, so the first component will be the amplitude of the light in the horizontal cavity mode and the second component will be the amplitude of the light in the vertical cavity mode.

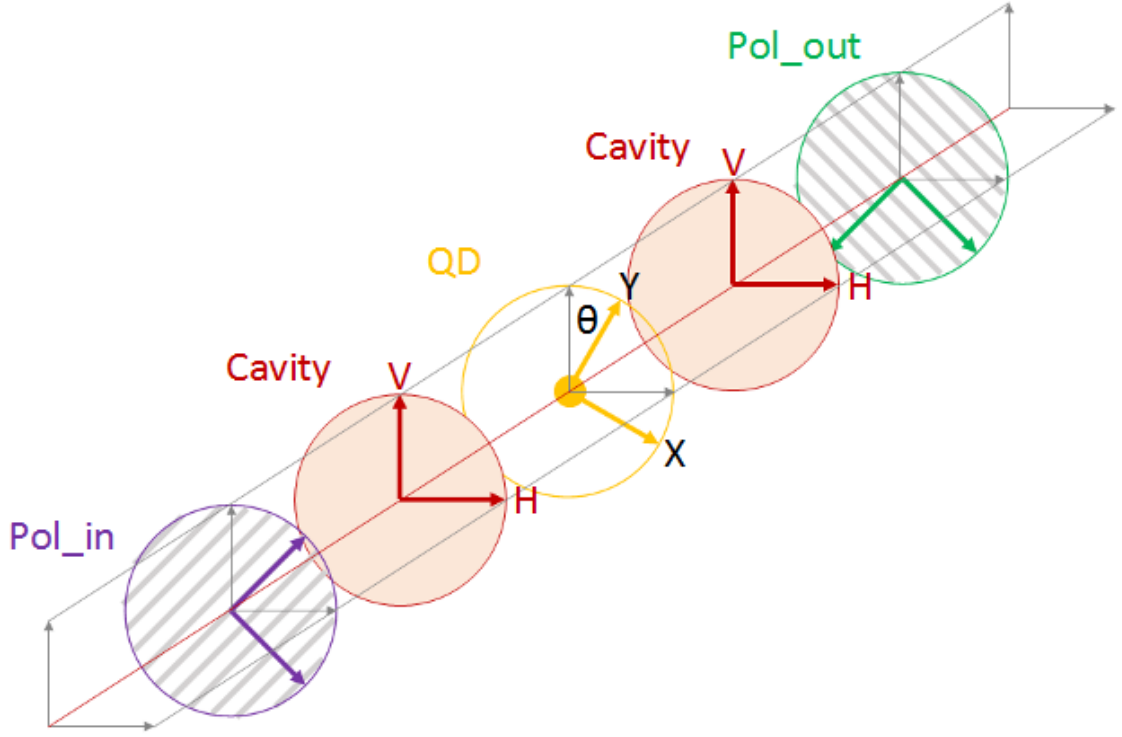


**Figure 2.5:** A schematic overview of the axes involved. Through the use of linear polarisers and waveplates we can fix the input polarization and filter the output polarization. The optical cavity is polarization non-degenerate with eigenmodes ‘H’ and ‘V’, the quantum dot is polarization non-degenerate with eigenmodes ‘X’ and ‘Y’. The quantum dot angle  $\theta_{\text{QD}}$  is defined as the angle between these two sets of axes.

The light in the horizontal polarization picks up a phase  $i\Delta_H$  as before, and the light in the vertical polarization picks up the phase  $i\Delta_V$ . This can be written most easily as the diagonal matrix

$$\begin{pmatrix} i\Delta_H & 0 \\ 0 & i\Delta_V \end{pmatrix}.$$

Then the light interacts with the quantum dot. The easiest way to oversee this interaction is to rotate our polarization frame over the quantum dot angle  $\theta_{\text{QD}}$ . After this rotation the interaction can be written as a diagonal matrix with two Lorentzian lineshapes on the diagonal, leading to the contribution

$$-R_{-\theta_{\text{QD}}} \begin{pmatrix} \frac{2C}{1-i\Delta'_X} & 0 \\ 0 & \frac{2C}{1-i\Delta'_Y} \end{pmatrix} R_{\theta_{\text{QD}}}$$

where

$$R_{\theta_{\text{QD}}} = \begin{pmatrix} \cos(\theta_{\text{QD}}) & -\sin(\theta_{\text{QD}}) \\ \sin(\theta_{\text{QD}}) & \cos(\theta_{\text{QD}}) \end{pmatrix}$$

is the rotation matrix. Aside from losses, which are incorporated in the global efficiency parameter  $\eta_{\text{out}}$ , this is the only interaction the light has per round trip. Therefore our amplitude

vector is transformed after one round trip as

$$\mathbf{e}_1 = \left( I_{2 \times 2} + \begin{pmatrix} i\Delta_H & 0 \\ 0 & i\Delta_V \end{pmatrix} - R_{-\theta_{\text{QD}}} \begin{pmatrix} \frac{2C}{1-i\Delta'_X} & 0 \\ 0 & \frac{2C}{1-i\Delta'_Y} \end{pmatrix} R_{\theta_{\text{QD}}} \right) \mathbf{e}_0.$$

Here we have used a first-order Taylor approximation, turning the multiplication of these two effects on the amplitude into an addition. This approximation is allowed since we are interested in the behaviour of this system near resonance, so all detunings involved are small. We can repeat this process to find the amplitude vector after an arbitrary number of round trips. Summing over all round trips (so taking the amplitude vector after infinitely many round trips) now gives us the steady state amplitude transmission matrix

$$\begin{aligned} t_{2 \times 2} &= \eta_{\text{out}} \sum_{n=0}^{\infty} \left( \begin{pmatrix} i\Delta_H & 0 \\ 0 & i\Delta_V \end{pmatrix} - R_{-\theta_{\text{QD}}} \begin{pmatrix} \frac{2C}{1-i\Delta'_X} & 0 \\ 0 & \frac{2C}{1-i\Delta'_Y} \end{pmatrix} R_{\theta_{\text{QD}}} \right)^n \\ &= \eta_{\text{out}} \left( I_{2 \times 2} - \begin{pmatrix} i\Delta_H & 0 \\ 0 & i\Delta_V \end{pmatrix} + R_{-\theta_{\text{QD}}} \begin{pmatrix} \frac{2C}{1-i\Delta'_X} & 0 \\ 0 & \frac{2C}{1-i\Delta'_Y} \end{pmatrix} R_{\theta_{\text{QD}}} \right)^{-1}. \end{aligned}$$

This generalises the single polarization mode result presented earlier and allows us to numerically compute the transmission of a polarization non-degenerate cavity system.

## 2.2.2 Interpreting the transmission matrix

The semiclassical model is not capable of simulating the indistinguishability of the single photons. However, the intensities of the light being transmitted through the cavity do give us some insight into the brightness and purity of this single photon source. This means that we can deduce criteria for good SPS characteristics from the semiclassical model. Section 3 gives a quantitative analysis of this statement, deriving an expression for the purity of a SPS in terms of output intensities in a classical optics setting. In this section we will explain which constraints on the polarization will generate good single photon sources.

With the transmission matrix above we can simulate an empty cavity by setting the quantum dot detunings,  $\Delta'_X$  and  $\Delta'_Y$ , to very large numbers, in which case the quantum dot interaction vanishes and we are only considering a polarization non-degenerate empty cavity. Through controlling input and output polarisers we will search for configurations with maximum intensity in the presence of a QD (on a scale of 0 to  $\eta_{\text{out}}$ ) and minimum intensity in the absence of the quantum dot.

In order to have this system function as a reasonable SPS the output needs to almost exclusively consist of single photons. It is therefore important that the output polarization is chosen such that the coherent light passing through the empty cavity is nearly 0, i.e. we need to choose an input polarization vector  $\mathbf{e}_{in}$  and an output polarization filter  $\mathbf{e}_{out}$  such that  $\langle \mathbf{e}_{out}, t_{2 \times 2, \text{noQD}} \cdot \mathbf{e}_{in} \rangle \approx 0$ . Since every input polarization will produce some output polarization  $t_{2 \times 2, \text{noQD}} \cdot \mathbf{e}_{in}$ , which has a unique (up to a global phase) orthogonal polarization, this means that once we fix the input polarization we are left with no degrees of freedom for the output polariser if we want high purity. At the same time it means that at least theoretically it is

possible to obtain perfect purity through the use of polarizers and quarter wave plates alone (for a specific frequency). Since we can therefore always ensure that our configuration has high purity, the condition that separates good choices of polarization from bad ones in our setup is the intensity (brightness) of the SPS, which we can influence through the remaining degrees of freedom of the input polariser.

To better understand the brightness of the SPS in this setup it is interesting to consider the most simple ‘90Cross’ configuration, where the input polarization is set to one of the two cavity modes (say H) and the polarization filter in the outgoing path is set to the other, orthogonal, polarization mode (say V). This clearly meets the orthogonality requirement explained above – in the absence of a quantum dot the cavity does not alter the polarization of the incoming light at all, and it is completely dimmed before reaching the detector. But to see why this configuration is usually not optimal for brightness it is important to consider the quantum dot interaction term in more detail. We expand:

$$R_{-\theta_{\text{QD}}} \begin{pmatrix} \frac{2C}{1-i\Delta'_X} & 0 \\ 0 & \frac{2C}{1-i\Delta'_Y} \end{pmatrix} R_{\theta_{\text{QD}}} = \begin{pmatrix} \cos^2(\theta_{\text{QD}}) \frac{2C}{1-i\Delta'_X} + \sin^2(\theta_{\text{QD}}) \frac{2C}{1-i\Delta'_Y} & \cos(\theta_{\text{QD}}) \sin(\theta_{\text{QD}}) \left( \frac{2C}{1-i\Delta'_Y} - \frac{2C}{1-i\Delta'_X} \right) \\ \cos(\theta_{\text{QD}}) \sin(\theta_{\text{QD}}) \left( \frac{2C}{1-i\Delta'_Y} - \frac{2C}{1-i\Delta'_X} \right) & \cos^2(\theta_{\text{QD}}) \frac{2C}{1-i\Delta'_Y} + \sin^2(\theta_{\text{QD}}) \frac{2C}{1-i\Delta'_X} \end{pmatrix}.$$

Now generally the spectral linewidth of the quantum dot modes is sufficiently narrow that they do not overlap, so for any fixed frequency at least one of  $\Delta'_X$  and  $\Delta'_Y$  is very large. Assuming in this example that we tune the laser on-resonance with the X quantum dot mode we omit the terms containing  $\Delta'_Y$  and find

$$R_{-\theta_{\text{QD}}} \begin{pmatrix} \frac{2C}{1-i\Delta'_X} & 0 \\ 0 & 0 \end{pmatrix} R_{\theta_{\text{QD}}} = \frac{2C}{1-i\Delta'_X} \begin{pmatrix} \cos^2(\theta_{\text{QD}}) & -\frac{1}{2} \sin(2\theta_{\text{QD}}) \\ -\frac{1}{2} \sin(2\theta_{\text{QD}}) & \sin^2(\theta_{\text{QD}}) \end{pmatrix}.$$

These four matrix elements have clear physical interpretation: the top left element represents the amplitude of light in the H mode exciting the X quantum dot mode, which then emits back in the H cavity mode. Similarly, the process that is detected in the 90Cross configuration is given by the bottom left element – light in the H cavity mode exciting the X quantum dot mode and emitting in the V cavity mode. Important to observe is that the process of the QD emitting in the same cavity mode that excited it occurs proportionally to  $\cos^4(\theta_{\text{QD}})$  (since the above coefficients are amplitudes) or  $\sin^4(\theta_{\text{QD}})$ , whereas the process where a QD emits in the different cavity mode occurs proportionally to  $\frac{1}{4} \sin^2(2\theta_{\text{QD}})$ . For values of the QD angle  $\theta_{\text{QD}}$  close to 0 or 90 degrees (the QD angle has a 180 degree symmetry) the term  $\sin(2\theta_{\text{QD}})$  vanishes and the 90Cross configuration is a very poor choice for a SPS. Conversely even at the most extreme value of  $\theta_{\text{QD}} = 45$  degrees we still have  $\frac{1}{2} \sin(2\theta_{\text{QD}}) = 0.5 = \cos^2(\theta_{\text{QD}}) = \sin^2(\theta_{\text{QD}})$ , so even at the most convenient QD angle for this diagonal emission process it is still only as prevalent as re-emission into the original mode. It is therefore important to ensure that, while the polarising filter in the outgoing path is perpendicular to the emitted polarization of the empty cavity  $\mathbf{e}_{noQD}$ , it is not perpendicular to the ingoing polarization, because most of the QD light will be emitted in this same polarization. *This means that in an optimal configuration it is necessary that the empty cavity changes the polarization of the light – i.e.*

*the cavity needs to be polarization non-degenerate.*

If the cavity is polarization non-degenerate then, after fixing the input laser frequency, the transmitted light will pick up a different phase in the two cavity polarization modes, effectively causing the cavity to act like a birefringent crystal. Simulations and experiment below show us that the difference in phase picked up can be as large as  $90^\circ$ , giving us a lot of control over the desired output polarization.

Armed with the knowledge that we need to make use of the birefringent properties of the empty cavity we are forced to choose an input polarization that has non-zero amounts of light in both cavity polarization modes. For simplicity we consider the case where the laser frequency is set precisely between the two cavity modes, so  $\Delta_H = -\Delta_V$ . In the absence of the QD the transmission matrix now simplifies to

$$t_{2 \times 2, \text{noQD}} = \left( I_{2 \times 2} + \begin{pmatrix} i\Delta_H & 0 \\ 0 & i\Delta_V \end{pmatrix} \right)^{-1} = \begin{pmatrix} \frac{1}{1-i\frac{\Delta_{\text{Cav}}}{2}} & 0 \\ 0 & \frac{1}{1+i\frac{\Delta_{\text{Cav}}}{2}} \end{pmatrix}.$$

with  $\Delta_{\text{Cav}}$  the (normalised) splitting in frequency between the two cavity modes. If in these normalised coordinates the cavity is split such that  $\Delta_{\text{Cav}} = 2$  then a diagonal input polarization  $\mathbf{e}_{in} = \frac{1}{\sqrt{2}} \begin{pmatrix} 1 \\ 1 \end{pmatrix}$  gives us a completely circular output polarization  $\mathbf{e}_{out} = t_{2 \times 2, \text{noQD}} \mathbf{e}_{in} = \frac{1+i}{2} \frac{1}{\sqrt{2}} \begin{pmatrix} 1 \\ i \end{pmatrix}$ . In our sample the splitting between the cavity modes is close to  $\Delta_{\text{Cav}} = 2$ . In this configuration the input polarization is diagonal, as specified above. The polarization filter in the outgoing path would be of the opposite circular polarization to the one emitted by the empty cavity. This configuration, which we denoted by ‘45Circ’, has the significant advantage over the 90Cross configuration that the output polariser is not perpendicular to the input polariser, so a large portion of the single photons re-emitted into the cavity mode that excited the quantum dot will pass through the output polariser and go to the detector. Furthermore this configuration has the advantage of being relatively easy to assemble experimentally, requiring only a polariser and a half wave plate on the input side of the sample and a polariser and a quarter wave plate on the output side.

Lastly, to find the truly optimal polarization configuration, the author and Marnix van de Stolpe have collaborated on writing an optimization algorithm that simulates the transmission through the cavity and generates optimal polarization configurations for single photon sources. For an extensive review of this algorithm we refer the reader to [23].



## $g^2(0)$ of mixed sources of light

In the previous sections we have explained that the dip in the autocorrelation function  $g^2(\tau)$  at zero time displacement ( $\tau = 0$ ) is a measure of the purity of a single photon source. And indeed, a perfect single photon source would have a dip in  $g^2(\tau)$  all the way to 0, i.e.  $g^2(0) = 0$ . In actual experiment there are two major obstacles that prevent us from detecting a  $g^2$ -dip all the way down to 0. The first is the detector response function, describing the imperfections of the detector (in particular the detector jitter). This has a significant influence on the observed autocorrelation function. The second contributing factor is the presence of a low amount of photons from the laser in the detection path. In this section we will explore the influence of these photons on the value of  $g^2(0)$  in both a quantum optics and a modified classical optics framework. To do this we will model a continuous wave monochromatic laser and mix it with the light emitted by a quantum dot. In section 5.3.1 we briefly discuss whether this approach is also valid if the pulsed laser is pulsed instead of continuous.



### 3.1 Quantum optical description of $g^2(0)$

In the framework of quantum optics the value of the second-order autocorrelation function at zero time displacement,  $g^2(0)$ , is given by the expression

$$g_{\phi}^2(0) = \frac{\langle \phi | \hat{a}^{\dagger} \hat{a}^{\dagger} \hat{a} \hat{a} | \phi \rangle}{|\langle \phi | \hat{a}^{\dagger} \hat{a} | \phi \rangle|^2}.$$

Here  $\phi$  is the state of the light in the detection arm and  $\hat{a}$  is the annihilation operator of a single photon at the frequency of our interest.

The value  $g^2(0)$  is normalised to the intensity squared of the state, which ensures that this autocorrelation dip is independent of losses or intensity gain and is therefore macroscopically observable.

We wish to model the value of  $g^2(0)$  of an outgoing light beam that is created by mixing two input beams. Of course if this problem is solved in full generality the result can be applied iteratively to mix arbitrary numbers of input beams. However we will restrict our analysis by assuming that the light emitted from the cavity is a mixture of pure single photons from the quantum dot, along with a low intensity contribution from the excitation laser. To model this mixing we use a beam splitter with amplitude transmission coefficient  $t$  and reflection coefficient  $r$ . In terms of the annihilation operators of the input arms ( $\hat{a}_1, \hat{a}_2$ ) and output arms ( $\hat{b}_1, \hat{b}_2$ ) the effect of the beam splitter can be written as

$$\begin{pmatrix} \hat{b}_1 \\ \hat{b}_2 \end{pmatrix} = \begin{pmatrix} t & r \\ -r & t \end{pmatrix} \begin{pmatrix} \hat{a}_1 \\ \hat{a}_2 \end{pmatrix}.$$

Where we demand that the transformation matrix is unitary, and we take  $t, r$  real with  $t^2 + r^2 = 1$ . The choice of  $t$  real is free of conditions, whereas the choice of  $r$  real corresponds to a choice of global phase difference between the two input arms of exactly  $90^\circ$ . We will work in the Fock basis to simplify working with single photons. The input state in the first arm is a single photon, given by  $|1\rangle = \hat{a}_1^\dagger|0\rangle$ . The state in the second input arm is coherent light, characterised by a complex parameter  $\alpha$ . This state is given by  $|\alpha\rangle = \exp(\alpha\hat{a}_2^\dagger - \alpha^*\hat{a}_2)|0\rangle$ . Using our conversion matrix for the beamsplitter above we find  $\hat{a}_1 = t\hat{b}_1 - r\hat{b}_2$ ,  $\hat{a}_2 = r\hat{b}_1 + t\hat{b}_2$  so

$$\begin{aligned} |\psi\rangle &= \hat{a}_1^\dagger \exp(\alpha\hat{a}_2^\dagger - \alpha^*\hat{a}_2)|0_1\rangle|0_2\rangle \\ &= (t\hat{b}_1^\dagger - r\hat{b}_2^\dagger) \exp(\alpha(r\hat{b}_1^\dagger + t\hat{b}_2^\dagger) - \alpha^*(r\hat{b}_1 + t\hat{b}_2))|0_1\rangle|0_2\rangle \\ &= (t\hat{b}_1^\dagger - r\hat{b}_2^\dagger) \exp(\alpha r\hat{b}_1^\dagger - \alpha^* r\hat{b}_1) \exp(\alpha t\hat{b}_2^\dagger - \alpha^* t\hat{b}_2)|0_1\rangle|0_2\rangle. \end{aligned}$$

Where we split the exponential and used that the creation and annihilation operators with different indices commute. We now wish to move the exponential containing  $\hat{b}_2$  all the way to the left. To do this we will first split it in two parts, and then move these to the left separately. So:

$$\exp(\alpha t\hat{b}_2^\dagger - \alpha^* t\hat{b}_2) = \exp(-|t\alpha|^2/2) \exp(\alpha t\hat{b}_2^\dagger) \exp(-\alpha^* t\hat{b}_2).$$

The first two exponents commute with  $\hat{b}_1$ ,  $\hat{b}_1^\dagger$  and  $\hat{b}_2^\dagger$  and can therefore immediately be moved to the left. The second term commutes with  $\hat{b}_1$  and  $\hat{b}_1^\dagger$  but not with  $\hat{b}_2^\dagger$ , so we compute:

$$\begin{aligned} [\hat{b}_2^\dagger, \exp(-\alpha^* t \hat{b}_2)] &= \sum_{n=0}^{\infty} \frac{(-\alpha^* t)^n}{n!} [\hat{b}_2^\dagger, \hat{b}_2^n] \\ &= \sum_{n=0}^{\infty} \frac{(-\alpha^* t)^n}{n!} (-n \hat{b}_2^{n-1}) \\ &= -(-\alpha^* t) \sum_{n=1}^{\infty} \frac{(-\alpha^* t)^{n-1}}{(n-1)!} \hat{b}_2^{n-1} \\ &= \alpha^* t \exp(-\alpha^* t \hat{b}_2). \end{aligned}$$

So we find that

$$\begin{aligned} (t\hat{b}_1^\dagger - r\hat{b}_2^\dagger) \exp(\alpha t \hat{b}_2^\dagger - \alpha^* t \hat{b}_2) &= (t\hat{b}_1^\dagger - r\hat{b}_2^\dagger) \exp(-|t\alpha|^2/2) \exp(\alpha t \hat{b}_2^\dagger) \exp(-\alpha^* t \hat{b}_2) \\ &= \exp(-|t\alpha|^2/2) \exp(\alpha t \hat{b}_2^\dagger) (t\hat{b}_1^\dagger - r\hat{b}_2^\dagger) \exp(-\alpha^* t \hat{b}_2) \\ &= \exp(-|t\alpha|^2/2) \exp(\alpha t \hat{b}_2^\dagger) \exp(-\alpha^* t \hat{b}_2) (t\hat{b}_1^\dagger - r\hat{b}_2^\dagger - r\alpha^* t) \\ &= \exp(\alpha t \hat{b}_2^\dagger - \alpha^* t \hat{b}_2) (t\hat{b}_1^\dagger - r\hat{b}_2^\dagger - r\alpha^* t). \end{aligned}$$

So that also

$$\begin{aligned} |\psi\rangle &= (t\hat{b}_1^\dagger - r\hat{b}_2^\dagger) \exp(\alpha r \hat{b}_1^\dagger - \alpha^* r \hat{b}_1) \exp(\alpha t \hat{b}_2^\dagger - \alpha^* t \hat{b}_2) |0_1\rangle |0_2\rangle \\ &= \exp(\alpha t \hat{b}_2^\dagger - \alpha^* t \hat{b}_2) (t\hat{b}_1^\dagger - r\hat{b}_2^\dagger - r\alpha^* t) \exp(\alpha r \hat{b}_1^\dagger - \alpha^* r \hat{b}_1) |0_1\rangle |0_2\rangle. \end{aligned}$$

At this point we remark that the leftmost operator is a unitary transformation acting only on the output of arm 2 - the output arm we are not interested in. This means that we may ignore it. More formally put, if  $\hat{O}_1$  is some operator acting only on the first output arm, i.e.  $[\hat{O}_1, \hat{b}_2] = [\hat{O}_1, \hat{b}_2^\dagger] = 0$ , and we write  $|\phi\rangle = (t\hat{b}_1^\dagger - r\hat{b}_2^\dagger - r\alpha^* t) \exp(\alpha r \hat{b}_1^\dagger - \alpha^* r \hat{b}_1) |0_1\rangle |0_2\rangle$  (which coincides with  $|\psi\rangle$  with the first exponent removed) then we have:

$$\begin{aligned} \langle \psi | \hat{O}_1 | \psi \rangle &= \langle \psi | \hat{O}_1 \exp(\alpha t \hat{b}_2^\dagger - \alpha^* t \hat{b}_2) (t\hat{b}_1^\dagger - r\hat{b}_2^\dagger - r\alpha^* t) \exp(\alpha r \hat{b}_1^\dagger - \alpha^* r \hat{b}_1) |0_1\rangle |0_2\rangle \\ &= \langle \psi | \exp(\alpha t \hat{b}_2^\dagger - \alpha^* t \hat{b}_2) \hat{O}_1 (t\hat{b}_1^\dagger - r\hat{b}_2^\dagger - r\alpha^* t) \exp(\alpha r \hat{b}_1^\dagger - \alpha^* r \hat{b}_1) |0_1\rangle |0_2\rangle \\ &= \langle \phi | \hat{O}_1 | \phi \rangle. \end{aligned}$$

Since we are interested only in expressions for  $\hat{O}_1$  consisting entirely of products of  $\hat{b}_1$  and  $\hat{b}_1^\dagger$  we can therefore continue to consider only  $|\phi\rangle$  instead of  $|\psi\rangle$ . We will first compute the denominator of our expression for  $g^2(0)$ . To compute this we remark that  $|\phi\rangle$  written in the double Fock basis  $|n_1\rangle |n_2\rangle$  only has non-zero amplitudes whenever  $n_2 = 0, 1$ . We write

$$|\phi\rangle = \sum_{n=0}^{\infty} \sum_{m=0}^1 A_{n,m} |n_1\rangle |m_2\rangle.$$

Our expression for  $|\phi\rangle$  now gives

$$\begin{aligned} |\phi\rangle &= (t\hat{b}_1^\dagger - r\hat{b}_2^\dagger - r\alpha^*t) \exp(\alpha r\hat{b}_1^\dagger - \alpha^*r\hat{b}_1)|0_1\rangle|0_2\rangle \\ &= \exp(-|r\alpha|^2/2)(t\hat{b}_1^\dagger - r\hat{b}_2^\dagger - r\alpha^*t) \sum_{n=0}^{\infty} \frac{(r\alpha)^n}{\sqrt{n!}} |n_1\rangle|0_2\rangle \\ &= \exp(-|r\alpha|^2/2) \left( t \sum_{n=0}^{\infty} \frac{(r\alpha)^n}{\sqrt{n!}} \sqrt{n+1} |n+1_1\rangle|0_2\rangle - r \sum_{n=0}^{\infty} \frac{(r\alpha)^n}{\sqrt{n!}} |n_1\rangle|1_2\rangle - r\alpha^*t \sum_{n=0}^{\infty} \frac{(r\alpha)^n}{\sqrt{n!}} |n_1\rangle|0_2\rangle \right). \end{aligned}$$

Now we introduce the probabilities of finding  $n$  photons in output arm 1, given by  $Z_n = |A_{n,0}|^2 + |A_{n,1}|^2$ . From the expression above we find that:

$$\begin{aligned} Z_n &= \begin{cases} \exp(-|r\alpha|^2)(r^2 + r^2|\alpha|^2t^2) & n = 0 \\ \exp(-|r\alpha|^2) \left( r^2 \frac{|r\alpha|^{2n}}{n!} + \frac{|r\alpha|^{2(n-1)}}{(n-1)!} \left| t\sqrt{n} - r\alpha^*t \frac{r\alpha}{\sqrt{n}} \right|^2 \right) & n > 0 \end{cases} \\ &= \begin{cases} \exp(-|r\alpha|^2)(r^2 + r^2|\alpha|^2t^2) & n = 0 \\ \exp(-|r\alpha|^2) \left( r^2 \frac{|r\alpha|^{2n}}{n!} + \frac{|r\alpha|^{2(n-1)}}{(n-1)!} (t^2n - 2t^2|\alpha|^2r^2 + r^2|\alpha|^2t^2 \frac{|r\alpha|^2}{n}) \right) & n > 0 \end{cases} \\ &= \begin{cases} \exp(-|r\alpha|^2)(r^2 + r^2|\alpha|^2t^2) & n = 0 \\ \exp(-|r\alpha|^2)(r^2 + r^2|\alpha|^2t^2) \frac{|r\alpha|^{2n}}{n!} + \exp(-|r\alpha|^2) \frac{|r\alpha|^{2(n-1)}}{(n-1)!} (t^2n - 2r^2|\alpha|^2t^2) & n > 0 \end{cases}. \end{aligned}$$

Note that for any operator  $\hat{O}_1$  acting only on the first output beam as before we have

$$\begin{aligned} \langle \phi | \hat{O}_1 | \phi \rangle &= \sum_{k=0}^{\infty} \sum_{l=0}^1 A_{k,l}^* \langle k_1 | \langle l_2 | \hat{O}_1 \sum_{n=0}^{\infty} \sum_{m=0}^1 A_{n,m} |n_1\rangle |m_2\rangle \\ &= \sum_{k,n=0}^{\infty} \sum_{l,m=0}^1 A_{k,l}^* A_{n,m} \langle k_1 | \hat{O}_1 |n_1\rangle \langle l_2 | m_2\rangle \\ &= \sum_{k,n=0}^{\infty} \sum_{m=0}^1 A_{k,m}^* A_{n,m} \langle k_1 | \hat{O}_1 |n_1\rangle. \end{aligned}$$

In the particular case that  $\hat{O}_1$  is the number operator  $\hat{b}_1^\dagger \hat{b}_1$  we have  $\langle k_1 | \hat{O}_1 |n_1\rangle = n\delta_{k,n}$ , and the above expression reduces to

$$\langle \phi | \hat{b}_1^\dagger \hat{b}_1 | \phi \rangle = \sum_{n=0}^{\infty} \sum_{m=0}^1 |A_{n,m}|^2 n = \sum_{n=0}^{\infty} Z_n n.$$

Similarly for  $\hat{O}_1 = \hat{b}_1^\dagger \hat{b}_1^\dagger \hat{b}_1 \hat{b}_1$  we have  $\langle k_1 | \hat{O}_1 |n_1\rangle = n(n-1)\delta_{k,n}$ , so

$$\langle \phi | \hat{b}_1^\dagger \hat{b}_1^\dagger \hat{b}_1 \hat{b}_1 | \phi \rangle = \sum_{n=0}^{\infty} Z_n n(n-1).$$

We now compute:

$$\begin{aligned}
\langle \phi | \hat{b}_1^\dagger \hat{b}_1 | \phi \rangle &= \sum_{n=0}^{\infty} Z_n n \\
&= \exp(-|r\alpha|^2) \left( (r^2 + r^2|\alpha|^2 t^2) \sum_{n=0}^{\infty} \frac{|r\alpha|^{2n}}{n!} n - 2r^2|\alpha|^2 t^2 \sum_{n=1}^{\infty} \frac{|r\alpha|^{2(n-1)}}{(n-1)!} n + t^2 \sum_{n=1}^{\infty} \frac{|r\alpha|^{2(n-1)}}{(n-1)!} n^2 \right) \\
&= \exp(-|r\alpha|^2) \left( (r^2 + r^2|\alpha|^2 t^2) |r\alpha|^2 \exp(|r\alpha|^2) - 2r^2|\alpha|^2 t^2 (1 + |r\alpha|^2) \exp(|r\alpha|^2) \right. \\
&\quad \left. + t^2 \exp(|r\alpha|^2) (|r\alpha|^4 + 3|r\alpha|^2 + 1) \right) \\
&= (r^2 + r^2|\alpha|^2 t^2) |r\alpha|^2 - 2r^2|\alpha|^2 t^2 (1 + |r\alpha|^2) + t^2 (|r\alpha|^4 + 3|r\alpha|^2 + 1) \\
&= |\alpha|^4 (t^2 r^4 - 2t^2 r^4 + t^2 r^4) + |\alpha|^2 (r^4 - 2r^2 t^2 + 3t^2) + t^2.
\end{aligned}$$

Unitarity of the beamsplitter means that  $t^2 + r^2 = 1$ , so the above reduces to

$$\langle \phi | \hat{b}_1^\dagger \hat{b}_1 | \phi \rangle = r^2 |\alpha|^2 + t^2.$$

This result has a simple interpretation: the average photon number of the output beam is  $r^2$  times that of the coherent state  $|\alpha\rangle$  plus  $t^2$  times that of a single photon state. To determine the numerator of our expression for  $g^2(0)$  we compute

$$\begin{aligned}
\langle \phi | \hat{b}_1^\dagger \hat{b}_1^\dagger \hat{b}_1 \hat{b}_1 | \phi \rangle &= \sum_{n=0}^{\infty} Z_n n(n-1) \\
&= \exp(-|r\alpha|^2) \left( (r^2 + r^2|\alpha|^2 t^2) \sum_{n=0}^{\infty} \frac{|r\alpha|^{2n}}{n!} n(n-1) - 2r^2|\alpha|^2 t^2 \sum_{n=1}^{\infty} \frac{|r\alpha|^{2(n-1)}}{(n-1)!} n(n-1) \right. \\
&\quad \left. + t^2 \sum_{n=1}^{\infty} \frac{|r\alpha|^{2(n-1)}}{(n-1)!} n^2(n-1) \right) \\
&= \exp(-|r\alpha|^2) \left( (r^2 + r^2|\alpha|^2 t^2) |r\alpha|^4 \exp(|r\alpha|^2) - 2r^2|\alpha|^2 t^2 |r\alpha|^2 (2 + |r\alpha|^2) \exp(|r\alpha|^2) \right. \\
&\quad \left. + t^2 \exp(|r\alpha|^2) |r\alpha|^2 (|r\alpha|^4 + 5|r\alpha|^2 + 4) \right) \\
&= (r^2 + r^2|\alpha|^2 t^2) |r\alpha|^4 - 2r^2|\alpha|^2 t^2 |r\alpha|^2 (2 + |r\alpha|^2) + t^2 |r\alpha|^2 (|r\alpha|^4 + 5|r\alpha|^2 + 4) \\
&= |\alpha|^6 (t^2 r^4 - 2t^2 r^4 + t^2 r^4) + |\alpha|^4 (r^6 - 4t^2 r^4 + 5t^2 r^4) + 4t^2 r^2 |\alpha|^2 \\
&= r^4 |\alpha|^4 + 4t^2 r^2 |\alpha|^2.
\end{aligned}$$

Introducing the intensity transmission and reflection coefficients  $T = t^2$ ,  $R = r^2$  now allows us to write the expression for  $g^2(0)$  as

$$\begin{aligned}
g^2(0) &= \frac{\langle \phi | \hat{b}_1^\dagger \hat{b}_1^\dagger \hat{b}_1 \hat{b}_1 | \phi \rangle}{\langle \phi | \hat{b}_1^\dagger \hat{b}_1 | \phi \rangle^2} \\
&= \frac{R^2 |\alpha|^4 + 4TR |\alpha|^2}{(R|\alpha|^2 + T)^2} \\
&= 1 - \frac{(R|\alpha|^2 + T)^2 - (R^2 |\alpha|^4 + 4TR |\alpha|^2)}{(R|\alpha|^2 + T)^2} \\
&= 1 - \frac{T^2 - 2TR |\alpha|^2}{(R|\alpha|^2 + T)^2}.
\end{aligned}$$

In our experiments the outgoing beam consists of mainly single photons. This means that  $R|\alpha|^2 \ll T$ . We will therefore ignore the second term in the numerator, and find

$$g^2(0) \approx 1 - \frac{T^2}{(R|\alpha|^2 + T)^2}.$$

Now we remark that the intensity of the outgoing beam is proportional to its mean photon number. This means that the total intensity of the outgoing beam with a QD in the cavity,  $I_{\text{withQD}}$ , can be written as  $I_{\text{withQD}} = I_0(R|\alpha|^2 + T)$ . Similarly the total intensity of the outgoing beam in the absence of a QD is proportional to the photon number of the laser, so  $I_{\text{noQD}} = I_0|\alpha|^2$ . From this we find that

$$\frac{I_{\text{withQD}}}{I_0} = R|\alpha|^2 + T = (1 - T) \frac{I_{\text{noQD}}}{I_0} + T = \frac{I_{\text{noQD}}}{I_0} + T(1 - |\alpha|^2).$$

So also  $T = \frac{1}{1-|\alpha|^2} \frac{I_{\text{withQD}} - I_{\text{noQD}}}{I_0} = \frac{1}{1-|\alpha|^2} \frac{\Delta I}{I_0}$ . Substituting this now gives

$$g^2(0) \approx 1 - \frac{T^2}{(R|\alpha|^2 + T)^2} = 1 - \frac{1}{(1 - |\alpha|^2)^2} \frac{(\Delta I)^2}{I_{\text{withQD}}^2}.$$

As a final step we remark that the  $g^2(0)$  of a single photon is 0 (as  $\langle 1 | \hat{b}_1^\dagger \hat{b}_1^\dagger \hat{b}_1 \hat{b}_1 | 1 \rangle = 0$ ) and the  $g^2(0)$  of coherent light is 1, so we can write the expression above in the more suggestive form

$$g^2(0) - 1 \approx \frac{(g_{|\alpha\rangle}^2(0) - 1)I_n^2 + (g_{|1\rangle}^2(0) - 1)\frac{1}{(1-|\alpha|^2)^2}(\Delta I)^2}{(I_{\text{noQD}} + \Delta I)^2}.$$

## 3.2 Classical $g^2(\mathbf{0})$

Classical optics also has a second-order autocorrelation function  $g^2(\tau)$ , the so-called intensity autocorrelation function, which is written in terms of the time-dependent intensity of the light as

$$g^2(\tau) = \frac{\frac{1}{t_{\text{max}}} \int_0^{t_{\text{max}}} I(t + \tau) I(t) dt}{\left( \frac{1}{t_{\text{max}}} \int_0^{t_{\text{max}}} I(t) dt \right)^2}.$$

Contrary to the quantum optical  $g^2(\tau)$  the classical definition guarantees that  $g^2(0) \geq 1$  (since the average value of  $I(t)^2$  is always at least the square of the average value of  $I(t)$ , by Jensen's inequality). This forms a problem since in the previous section we have explicitly worked with sources of light with a zero-time autocorrelation of less than 1. To mitigate this we will use the formula above to combine different sources of light, but will reduce the final expression to one explicitly dependent on the  $g^2(\tau)$  of the sources. This way we can manually input classically forbidden values of  $g^2(\tau)$ , while adhering to a classical description of the light.

To mix light in a classical setting we can simply add the electric fields of the different sources. We will assume that there is no definite phase relation between our single photon source and

our pump laser. This assumption is justified since the time at which the quantum dot decays is determined by its lifetime, and not by the external electric field. Because of this case we may even simply add the intensities of both sources to find the behaviour of the output beam. In particular we will introduce again the intensity of the light coming through an empty cavity,  $I_{\text{noQD}}(t)$ , and the light coming through a cavity with a quantum dot in it,  $I_{\text{withQD}}(t)$ , and their difference  $\Delta I(t) = I_{\text{withQD}}(t) - I_{\text{noQD}}(t)$ . Since the light from the pump laser is coherent it satisfies  $g_{\text{noQD}}^2(0) = 1$ . Since the difference in output between these two scenarios is created purely by the quantum dot, which has zero autocorrelation at time zero, we have  $g_{\text{SPS}}^2(0) = 0$ . The assumption of independence above guarantees that the intensities of the quantum dot and the pump are independent in time (which is the case for a continuous pump), i.e.  $\langle \Delta I(t) I_{\text{noQD}}(t) \rangle = \langle \Delta I(t) \rangle \langle I_{\text{noQD}}(t) \rangle$  (where the expectation value is taken in time, i.e.  $\langle X \rangle = \frac{1}{t_{\text{max}}} \int_0^t X(t) dt$ ). This gives us:

$$\begin{aligned}
g_{\text{total}}^2(\tau) &= \frac{\frac{1}{t_{\text{max}}} \int_0^{t_{\text{max}}} I_{\text{withQD}}(t) I_{\text{withQD}}(t + \tau) dt}{\left( \frac{1}{t_{\text{max}}} \int_0^{t_{\text{max}}} I_{\text{withQD}}(t) dt \right)^2} \\
&= \frac{\langle (I_{\text{noQD}} + \Delta I)(t) (I_{\text{noQD}} + \Delta I)(t + \tau) \rangle}{(\langle I_{\text{noQD}} + \Delta I \rangle)^2} \\
&= \frac{\langle I_{\text{noQD}}(t) I_{\text{noQD}}(t + \tau) + I_{\text{noQD}}(t) \Delta I(t + \tau) + I_{\text{noQD}}(t + \tau) \Delta I(t) + \Delta I(t) \Delta I(t + \tau) \rangle}{(\langle I_{\text{noQD}} \rangle + \langle \Delta I \rangle)^2} \\
&= \frac{\langle I_{\text{noQD}}(t) I_{\text{noQD}}(t + \tau) \rangle + \langle I_{\text{noQD}}(t) \Delta I(t + \tau) \rangle + \langle I_{\text{noQD}}(t + \tau) \Delta I(t) \rangle + \langle \Delta I(t) \Delta I(t + \tau) \rangle}{(\langle I_{\text{noQD}} \rangle + \langle \Delta I \rangle)^2} \\
&= \frac{\langle I_{\text{noQD}}(t) I_{\text{noQD}}(t + \tau) \rangle + 2 \langle I_{\text{noQD}} \rangle \langle \Delta I \rangle + \langle \Delta I(t) \Delta I(t + \tau) \rangle}{(\langle I_{\text{noQD}} \rangle + \langle \Delta I \rangle)^2}.
\end{aligned}$$

Now we use the fact that  $g_{\text{noQD}}^2(\tau) = \frac{\langle I_{\text{noQD}}(t) I_{\text{noQD}}(t + \tau) \rangle}{\langle I_{\text{noQD}} \rangle^2}$  and  $g_{\text{SPS}}^2(\tau) = \frac{\langle \Delta I(t) \Delta I(t + \tau) \rangle}{\langle \Delta I \rangle^2}$  to rewrite this as

$$\begin{aligned}
g_{\text{total}}^2(\tau) &= \frac{g_{\text{noQD}}^2(\tau) \langle I_{\text{noQD}} \rangle^2 + 2 \langle I_{\text{noQD}} \rangle \langle \Delta I \rangle + g_{\text{SPS}}^2(\tau) \langle \Delta I \rangle^2}{(\langle I_{\text{noQD}} \rangle + \langle \Delta I \rangle)^2} \\
&= 1 + \frac{(g_{\text{noQD}}^2(\tau) - 1) \langle I_{\text{noQD}} \rangle^2 + (g_{\text{SPS}}^2(\tau) - 1) \langle \Delta I \rangle^2}{(\langle I_{\text{noQD}} \rangle + \langle \Delta I \rangle)^2}.
\end{aligned}$$

Moving the 1 to the other side now gives a clear and insightful formula: the value of  $g^2(\tau) - 1$  of a mixture of two sources can be found by taking the values of  $g^2(\tau) - 1$  of each of the sources, weighing them by the square of the intensity of the source and adding them up. However it is important to note that we divide not by the sum of the squares of these intensities, but by the square of the sums. This means that the total denominator will always be more than the weights present in the numerator, and also that if we add a very large number of sources with comparable intensity the entire fraction becomes practically zero, implying that the  $g^2(\tau)$  of this mixture converges to 1 regardless of the character of the individual sources. This does not contradict the existence of macroscopic sources with  $g^2(\tau)$  different from the constant 1 function as we assume in our derivation that all these sources are independent, i.e. have no definite phase relation between the light they emit.

### 3.3 Comparison between the two

The two formulae are in great agreement, in fact the only difference is in the fraction  $\frac{1}{(1-|\alpha|^2)^2}$  at the end of the numerator. Since in practice we expect  $|\alpha|$  to be small this term is nearly equal to 1, and we may freely omit it for estimates. To further investigate this expression, assume that the light in our detection path consists of  $x$  parts coherent light leaked from the pump laser, and  $1-x$  part single photons created by the quantum dot, measured as fractions of the total intensity. Since the autocorrelation function is independent of total intensity we may divide by it, and we get the formula

$$g^2(0) - 1 = \frac{(1-x)x^2 + (0-x)(1-x)^2}{x + (1-x)} = -1 + 2x - x^2.$$

In the case that  $x$  is small, i.e. we have a good single photon source, we may further omit the term  $x^2$ , and find that  $g^2(0) \approx 2x$ . Therefore we can find the fraction of the light that is single photons by measuring the dip in the  $g^2(\tau)$  function, halving the value at the deepest point and taking the complement, i.e.

$$\text{Purity of a SPS} = 1 - \frac{g^2(0)}{2}.$$

Note that for this formula to be applicable to experimental results it is necessary to adjust for imperfections in the detector, as will be explained in more detail in the next section.

## Combining theory and experiment

In this section we will take a closer look at two aspects of the experimental setup that are important for replicating and interpreting the measurements, but did not appear in our theoretical analysis. The first of these two aspects concerns the origin of ‘leaked’ laser light in the detection path, while the second comments on the influences of an imperfect single photon detector on the experimentally observed  $g^2(\tau)$ -curve.

### 4.1 Leaked laser light

In the theoretical investigation of the semiclassical cavity model we determined that it is vital that the outgoing polariser filters the laser light that passes through the cavity without interacting with the quantum dot, to ensure that almost all of the light in the detection path of the setup indeed originates from the QD. We observe in practice that in the setup the peak height of the transmitted QD light is only roughly 1% of the total transmission through the cavity – meaning that if only one percent of the laser light passes through our output polariser the purity of the SPS is down to 50%. In practice we wish to detect very deep  $g^2(0)$ -dips, and the results from the previous section tell us that in order to detect (for example) a 80% dip the purity of the SPS needs to be around 90%, which translates to a polarization filter of 99.9% efficiency.

While the polarising filters have an erroneous transmission of approximately 0.001% as specified by the manufacturer, the main source of unwanted transmission is slight misalignment of the polariser angle. Since the intensity of the transmission in the perpendicular mode goes as  $\sin^2(\theta)$  with  $\theta$  the amount of misalignment this means that an erroneous angle of  $1^\circ$  translates to an intensity transmission of  $\sin^2(\theta) \approx 3 \times 10^{-4}$ , or a SPS purity of 97%. Despite the fact that this might seem like only a small deviation from a perfect SPS we can clearly detect purities this far away from 100% in our measurement, and misalignment by up to a single degree is likely present in the setup, so this is a significant contribution to the impurity of the SPS.

## 4.2 Detector response

Another mechanism which we have not considered in great detail is the workings of the single photon detectors and their influence on the observed autocorrelation function. Due to the normalisation of the  $g^2(\tau)$  function it is independent of losses, which means that reduced detector efficiency (and even asymmetric detector efficiency) have no influence on the observed autocorrelation curve other than increasing the amount of time needed to collect the histogram. However, an important deformation of the  $g^2(\tau)$  curve is created by the electronic jitter and electrical noise in the system processing the timestamps. Both of these contribute uncertainty to the timestamp of a single detection event. This uncertainty means that in our histogram of the coincidence counts all bins ‘flow over’ into the neighbouring bins. The effect of this is mathematically described as a convolution with the 2-time convoluted Detector Response Function, which is given in figure 4.1.

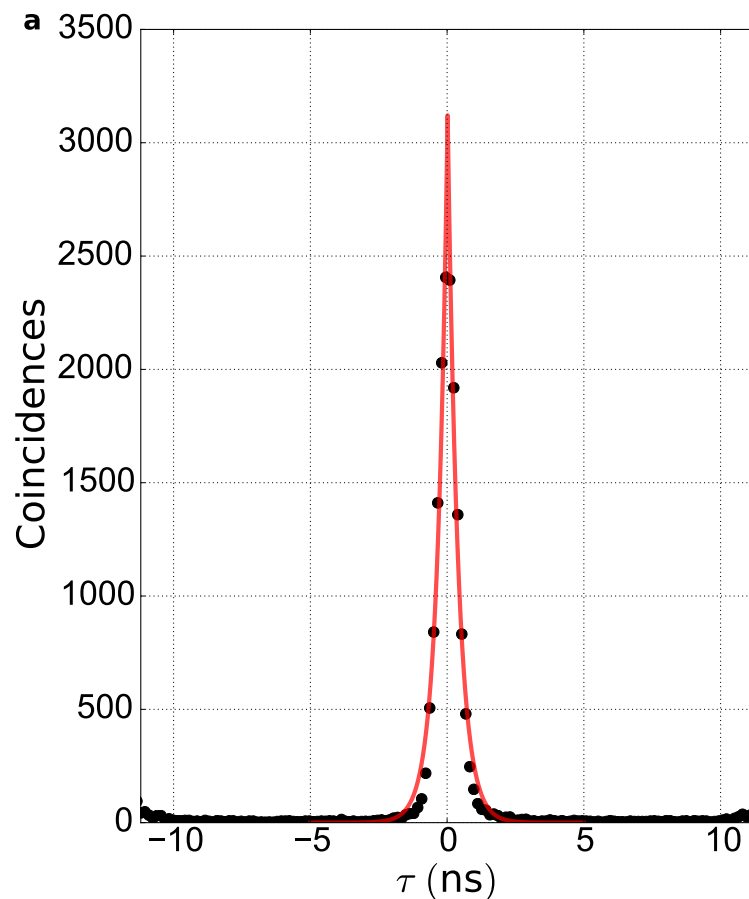


**Figure 4.1:** The 2-time convoluted detector response function, i.e. autocorrelation of a 50 ps laser pulse input. The experimental data (black) can be approximated well with a double exponential decay (red).

Since the  $g^2(\tau)$  dips we are looking for are narrow (in figure 2.2 we have shown the experimentally realistic FWHM of 6ns) this means that a significant amount of coincidences from outside the dip influence the deepest point, overall making the observed correlation function

less deep and wider. In this thesis we do not correct for this convolution, so it is important to keep in mind that the observed  $g^2(0)$ -values therefore only give (liberal) lower bounds on the purity of our SPS.

## 4.3 Simulations and measurements

In this section we will discuss the simulations and optimization algorithm for the semiclassical model of the polarization non-degenerate system. An extensive explanation of the workings of this model, along with the optimization settings, have already been presented in [23]. We will therefore focus particularly on predictions made by this simulation, and discuss the level of agreement between simulation and measurement.

The simulation determines the optimal polarization configuration for given parameters of the cavity and QD, and then proceeds to compute the transmitted light through the cavity for each of our three preferred polarization settings:

- ‘90Cross’, where the input polariser is aligned with a cavity axis and the output polarization filter aligned with the orthogonal cavity axis.
- ‘45Circ’, where the input polariser is aligned precisely  $45^\circ$  between the two cavity polarization modes and the output polariser filters circularly polarized light.
- ‘Optimal’, where the polarization settings are set (as close as possible) to the values found by the SPS optimization algorithm.

### 4.3.1 Theoretical predictions

The simulations predict that by tuning the polarisers away from the conventional ‘90Cross’ configuration we can achieve a higher brightness (intensity) of the SPS without losing purity. In particular for our cavity the ‘45Circ’ configuration should be both experimentally realisable and a significant improvement on the transmission intensity. On top of this a particular elliptical ‘Optimal’ polarization configuration, which is largely independent of the quantum dot properties, should give us maximal brightness of the SPS while maintaining high purity.

### 4.3.2 Comparison with measurement

In figure 4.2 below we present three lineshapes, i.e. graphs of the intensity of the transmission as a function of laser frequency, predicted by the simulation (top) above three measured lineshapes (below) for these same polarizations.

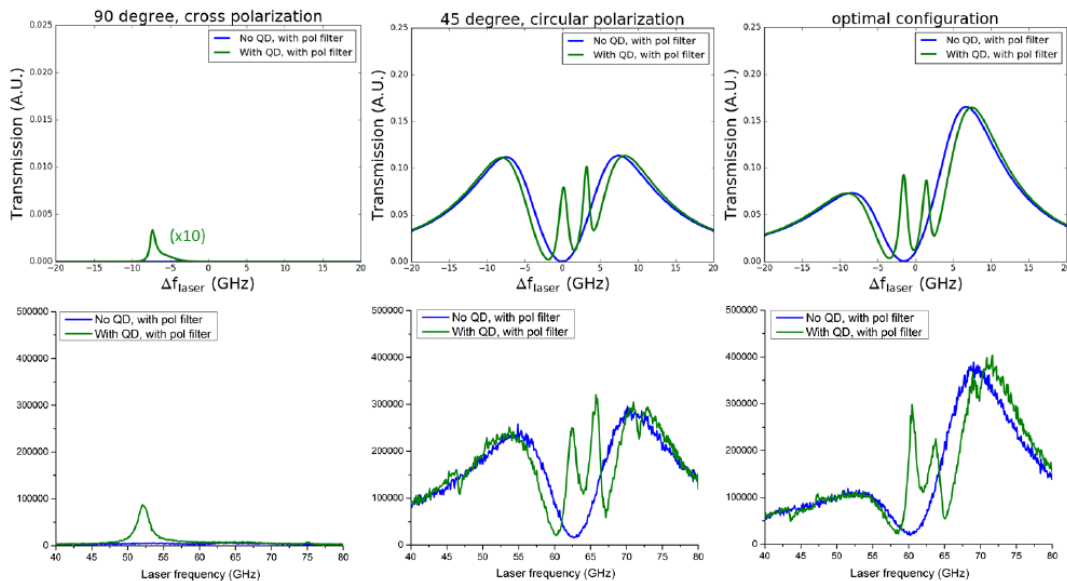


**Figure 4.2:** The transmission lineshapes for three different polarization configurations, simulated (top) and measured (bottom). Note that the vertical axis of the top left graph is a factor 10 lower than those of the other graphs in that column.

We see that there is remarkably good agreement between theory and experiment. The measured lineshapes, horizontal axes and height of the transmission peak by the QD agree closely with theory, leading the author to believe that this semiclassical model is an accurate simulation of our cavity. However, there are also some differences between the measured results and the theory that need to be addressed.

Firstly the QD emission in the ‘90Cross’ configuration is significantly higher in the measurement than was expected in theory (by roughly a factor 10). We believe that this is caused by the local electronic configuration around the QD. Note that the peak in the transmission for this measurement is shifted in frequency (52 GHz instead of 61 GHz) compared to the location of the peaks for the other two polarization configurations. To keep the QD on-resonance this means that we had to apply a different electric field for this particular measurement with the PIN junction, possibly giving rise to an unexpected local electronic reconfiguration [23].

Secondly the background transmission (lineshapes without the QD) in the ‘45Circ’ and ‘Optimal’ polarization configuration is not filtered by the output polarizer as well as predicted by the theory, visible as the non-zero background counts at the local minimum in these lineshapes. We have remarked before that the autocorrelation function is sensitive to the amount of background light present, so this limits the purity of the SPS severely. A possible reason for this is the also aforementioned sensitivity of the background on the precise angles of the waveplates and polarisers. While in this particular set of measurements the purity of the SPS in all three configurations are comparable, the low flat background in the ‘90Cross’ configuration allows for easier alignment of these optical instruments, explaining the relative lack of background in that experimental data.

Despite these discrepancies the semiclassical model gives us generally accurate predictions of the lineshapes observed experimentally. To test the predictions about the quality of the single photon source we proceed to determine the autocorrelation function  $g^2(\tau)$  in all three polarization configurations for a wide range of input laser power. Figure 4.3 shows a recently measured curve in the ‘90Cross’ configuration, along with a Lorentzian fit of the dip.

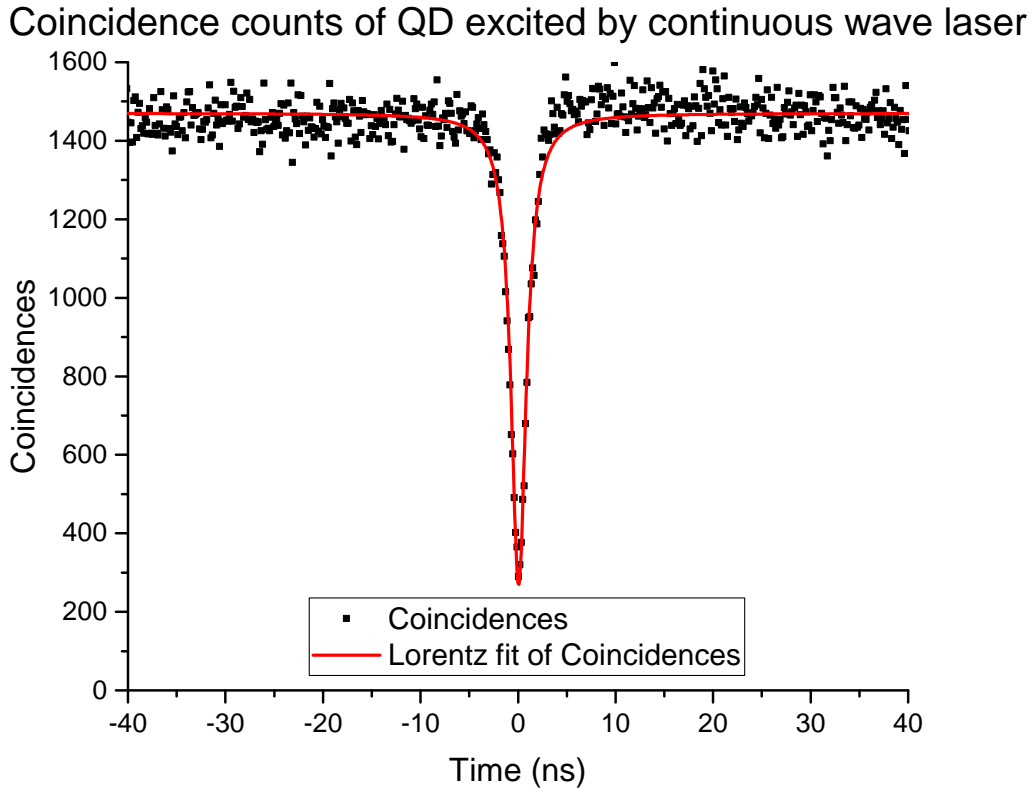


**Figure 4.3:** Experimentally determined autocorrelation function of a quantum dot excited by a continuous wave laser in the ‘90Cross’ configuration. The measured dip is  $g^2(0) \approx 19\%$ . Total measurement time was 200 seconds.

The measured autocorrelation function agrees well with the Lorentzian fit, and from this fit we can deduce the peak depth and therefore purity of this configuration. We present the measured dips in the  $g^2(\tau)$ -function plotted against the brightness of the SPS for all three polarization configurations in figure 4.4 below. We see that within the measurement error the dips for low counts (intensity) are comparable in all three polarization configurations, meaning that for low power all three polarization configurations produce SPS’s of comparable purity. However, the ‘45Circ’ and ‘Optimal’ configuration achieve higher count rate on the detector before the dip starts to decline (these configurations give us the same value of  $g^2(0)$  for higher output single counts). This agrees perfectly what was predicted by the theory: in the in the ‘45Circ’ configuration we can, at the same SPS purity, achieve higher brightness of the than in the ‘90Cross’ configuration, and in the ‘Optimal’ setting we can achieve a higher brightness still.

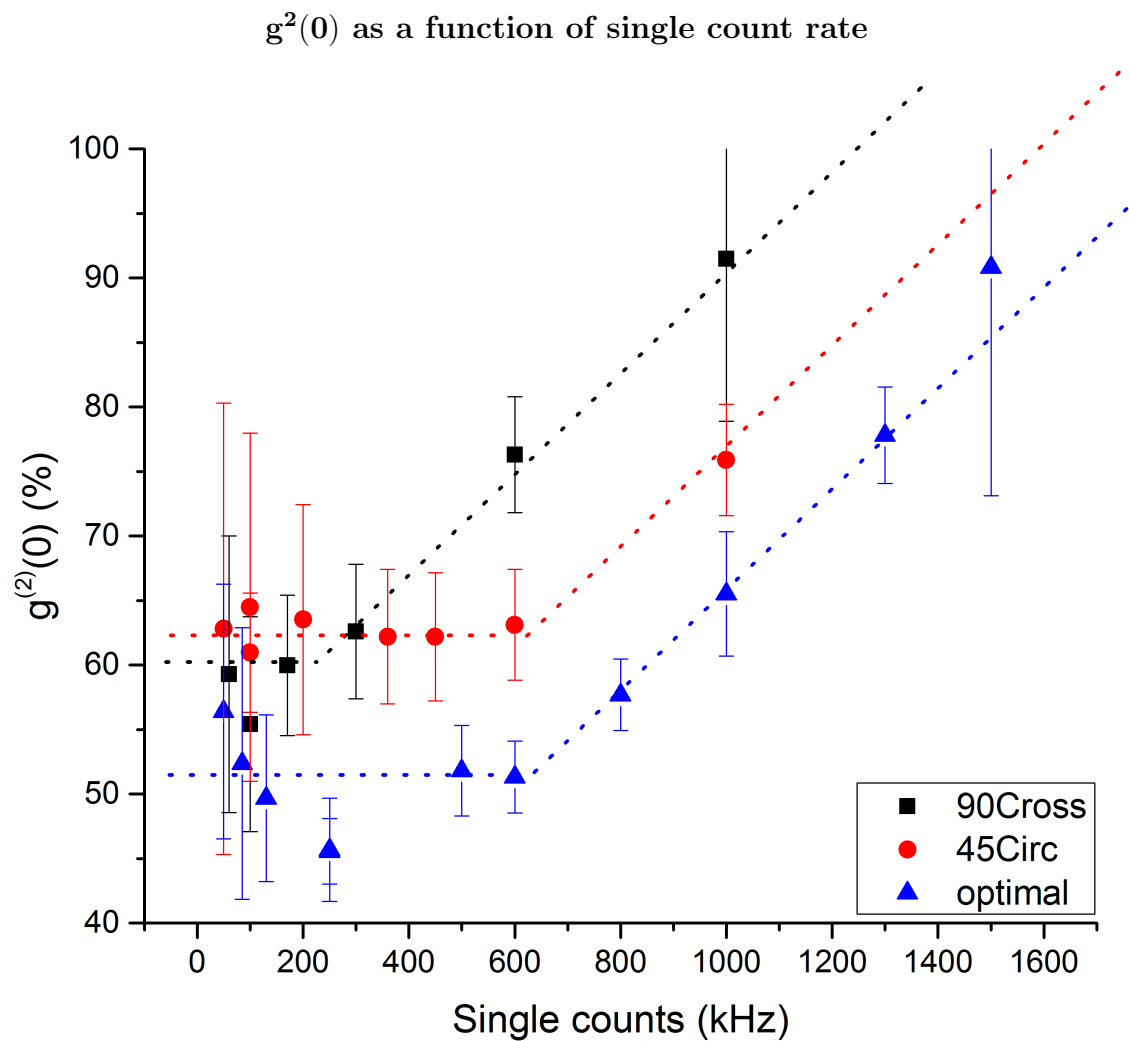


**Figure 4.4:** Lowest point (fitted) in the  $g^2(\tau)$ -curve plotted against the single count rate in one arm of the Hanbury-Brown-Twiss setup, for three different polarization configurations. The dotted lines guide the eye and are not fits.

## Rabi oscillations

In the previous sections we have seen that our semiclassical model produces accurate predictions for the behaviour of our polarization non-degenerate quantum dot in our polarization non-degenerate cavity. To further explore and classify the properties of our cavity QED setup we next looked experimentally for a well-established indicator of strong coupling to two-level systems; Rabi oscillations. We would like to mention at this point that such Rabi oscillations have only recently been observed in QD CQED systems [24–26] and there is great need to improve the understanding of the connected issues.

We will first briefly explain the theory of Rabi oscillations and then proceed to discuss what changes had to be made to the setup to detect the oscillations. Lastly we present our experimental results from this new setup and discuss the results.

### 5.1 Theory of Rabi oscillations

Rabi oscillations are a phenomenon where the number of single photons created by a quantum dot is not monotonic in the applied pump power, but rather oscillates as a function of the external electric field. To model the QD we remark that it is significantly smaller than the wavelength of the pump light (several nanometers versus 930 nm), so we can approximate it with an electrical dipole  $\hat{d}$ . The electric field applied by the laser as a function of time is given by  $\mathbf{E} \cos(\omega t)$  with  $\mathbf{E}$  the polarization and amplitude of the field and  $\omega = 2\pi \frac{\lambda}{c}$  the angular frequency of the light.

Writing  $|g\rangle$  for the ground state of the QD and  $|e\rangle$  for the excited state, the Hamiltonian of the QD is given by

$$H = |e\rangle\langle e| \hbar\omega_{\text{res}}$$

with  $\omega_{\text{res}} = \frac{E_e - E_g}{\hbar}$  the resonance frequency of the excitation of the quantum dot, which in our case coincides with the angular frequency  $\omega$  of the applied light (we excite the system on resonance). Note that we have here chosen an energy gauge where the ground state has zero energy.

Adding the laser light now introduces the interaction Hamiltonian  $\hat{V}_{\text{int}} = -\hat{d} \cdot \mathbf{E} \cos(\omega t) = \hat{V} \cos(\omega t)$  with  $\hat{V} = -\hat{d} \cdot \mathbf{E}$ . We will assume that  $\hat{V}$  has no diagonal terms – from the perspective

of perturbation theory the diagonal elements only change the energies of the ground and excited state, whereas the off-diagonal terms give rise to new behaviour. Writing the time-dependent state of the QD as  $\psi(t) = C_g(t)|g\rangle + C_e(t)e^{-i\omega_{\text{res}}t}|e\rangle$  and applying the Schrödinger equation with the Hamiltonian above now gives the equation

$$\begin{aligned} i\hbar \frac{\partial \psi}{\partial t} &= i\hbar \dot{C}_g(t)|g\rangle + i\hbar \left( \dot{C}_e(t)e^{-i\omega_{\text{res}}t} - i\omega_{\text{res}}C_e e^{-i\omega_{\text{res}}t} \right) |e\rangle \\ &= H(t)\psi \\ &= \left( \hbar\omega|e\rangle\langle e| + \hat{V} \cos(\omega t) \right) C_g(t)|g\rangle + C_e(t)e^{-i\omega_{\text{res}}t}|e\rangle \\ &= \left( C_e(t)e^{-i\omega_{\text{res}}t} \cos(\omega t) \langle g|\hat{V}|e\rangle \right) |g\rangle + \left( \hbar\omega C_e(t)e^{-i\omega_{\text{res}}t} + C_g(t) \cos(\omega t) \langle e|\hat{V}|g\rangle \right) |e\rangle. \end{aligned}$$

Collecting terms and writing  $\langle g|\hat{V}|e\rangle = V = \langle e|\hat{V}|g\rangle$  where we take this interaction term to be real gives us the coupled set of differential equations

$$\begin{aligned} \dot{C}_g &= -\frac{iV}{\hbar} e^{-i\omega t} \cos(\omega t) C_e \\ \dot{C}_e &= -\frac{iV}{\hbar} e^{i\omega t} \cos(\omega t) C_g. \end{aligned}$$

Next we expand the cosine in terms of exponentials and apply the so-called rotating wave approximation, where we discard terms oscillating very quickly and keep only the low-frequency contributions. This approximation is acceptable since the fast oscillations average out over any reasonable timescale that can be measured at, so they cannot be detected in our setup. Since  $\cos(\omega t) = \frac{e^{i\omega t} + e^{-i\omega t}}{2}$  we find

$$\begin{aligned} \dot{C}_g &= -\frac{iV}{2\hbar} C_e \\ \dot{C}_e &= -\frac{iV}{2\hbar} C_g. \end{aligned}$$

Putting these together in a second-order differential equation for  $C_e$  gives

$$\ddot{C}_e = -\frac{V^2}{4\hbar^2} C_e.$$

Assuming the QD started in the ground state, so  $C_g(0) = 1, C_e(0) = 0$  the solution to this is  $C_e(t) = -i \sin\left(\frac{V}{2\hbar}t\right)$ . In particular this means that the occupation of the excited state of the QD oscillates in time as  $|C_e(t)|^2 = \sin^2\left(\frac{V}{2\hbar}t\right)$ , which in turn also means that the amount of emitted photons oscillates in time (see figure 5.1). Or, more accurately, the amount of emitted photons oscillates with  $Vt$ . In our experiments we will keep the exposure time  $t$  fixed and change the value of  $V$  by changing the strength of the applied electric field  $\mathbf{E}$ , i.e. the applied laser power.

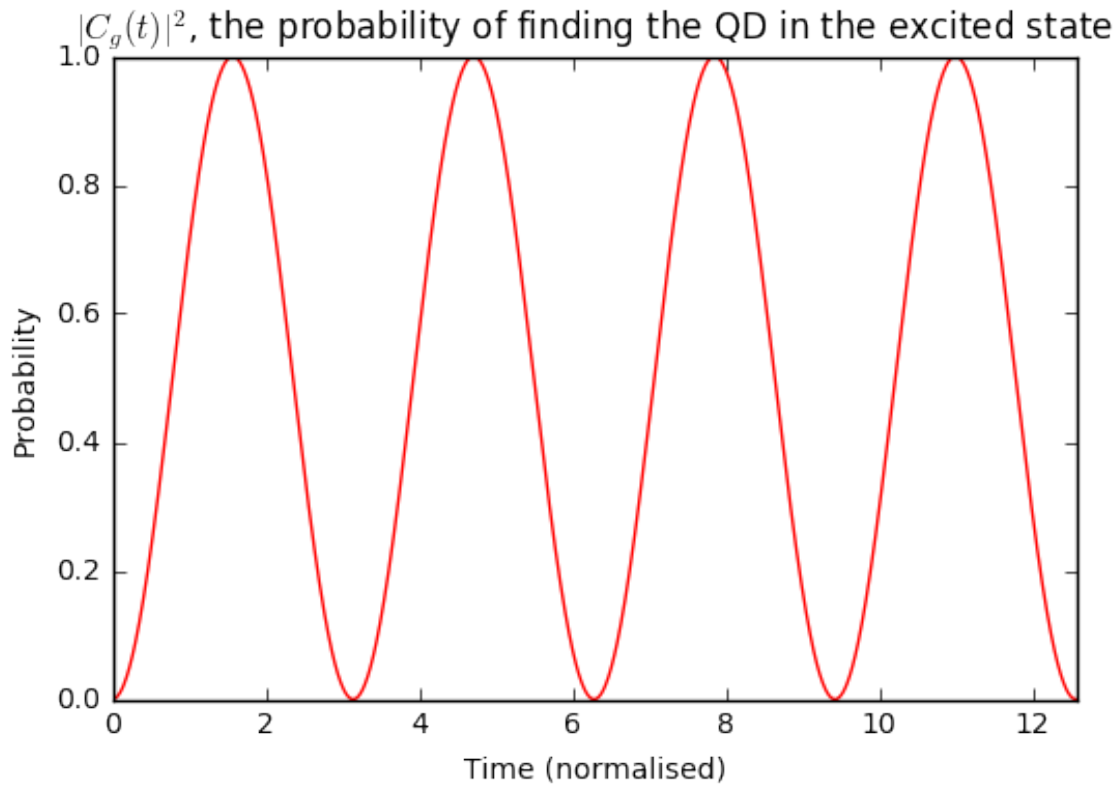


**Figure 5.1:** The probability of finding a two-level system in the excited state when applying an external on-resonance electric field. The simulated field strength corresponds to 2 nW inside the cavity.

In practice Rabi oscillations do not continue indefinitely, the amplitude of the Rabi oscillations decays exponentially due to dephasing (decoherence) of the quantum dot. We therefore expect that experimentally we will not see a clear oscillation as depicted in figure 5.1, but rather a damped oscillation as depicted in figure 5.2. In practice it is far more feasible to detect the first peak (corresponding to a  $\pi$ -pulse) than the higher order dips and peaks, so we are looking for a local maximum of the transmission intensity as a function of applied laser power.

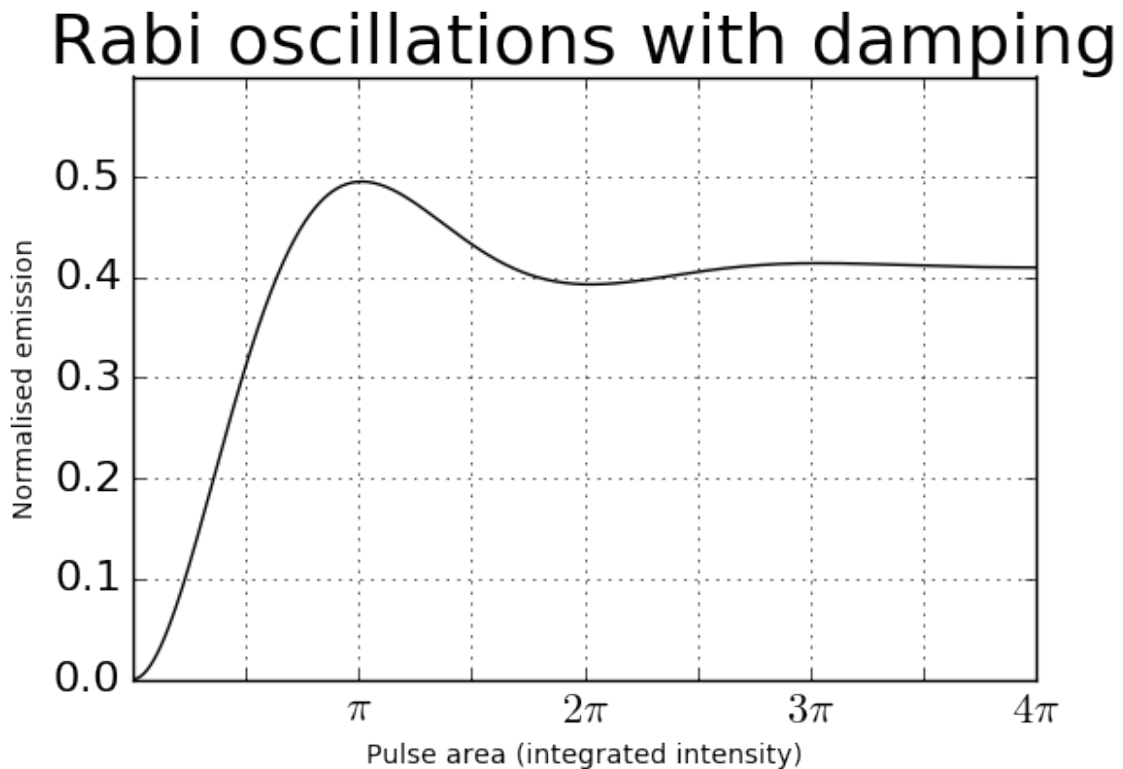


**Figure 5.2:** The transmission intensity as a function of pulse area, which is proportional to input laser intensity. In this simulation the QD decoherence decreases the amplitude of the oscillations. The damping rate in this simulation is set at one third of the Rabi frequency, so  $\gamma = \frac{1}{3}\Omega_R$ .

In cavity quantum electrodynamics the strength of the interaction between the quantum dot and the light in the cavity is given by the cooperativity  $C$ , which is the (dimensionless) average number of excitations of the quantum dot when inserting a single photon into the cavity. Note that in a cavity setup a photon can be absorbed by the quantum dot, emitted into the cavity mode and then re-absorbed by the quantum dot, so it is possible to have a value of  $C$  higher than 1. In our current sample the experimentally determined value of the cooperativity is approximately equal to 1. This means that the period of the Rabi oscillation is the same as the amount of time it takes to send a single photon into the cavity. To observe these Rabi oscillations we need to inject the light faster than the decay rate of the quantum dot, which is on the order of a single nanosecond. Injecting 1 photon of wavelength 930 nm every 0.1 nanosecond corresponds to a power of  $2 \times 10^{-9}$  W, or 2 nW inside the cavity.

## 5.2 Experimental design

To detect these Rabi Oscillations we wish to expose the sample to the laser light for a fixed amount of time and detect the number of single photons generated. This leads to two problems with the design of the setup, both of which can be fixed with a single change. Firstly to perform this experiment we need to have good (picosecond) control over the exposure time

of the sample. Secondly we have seen in the previous setup that applying high electric fields shifts the resonance frequency of the quantum dot and possibly has large impact on the local electronic configuration, so we cannot simply ramp up the power for this experiment [27]. We fix both these issues by performing this experiment with a pulsed laser, as opposed to a continuous wave laser. Since the pulse duration (50 ps) is very well defined this means that we have good control over the exposure time of the sample. Furthermore since the sample is not exposed continuously (but instead is exposed 50 ps per 12.5 ns) the average electric field in the cavity is very low, so we expect that there are no large shifts in the local electronic configuration.

Substituting a pulsed laser now gives us the following setup.

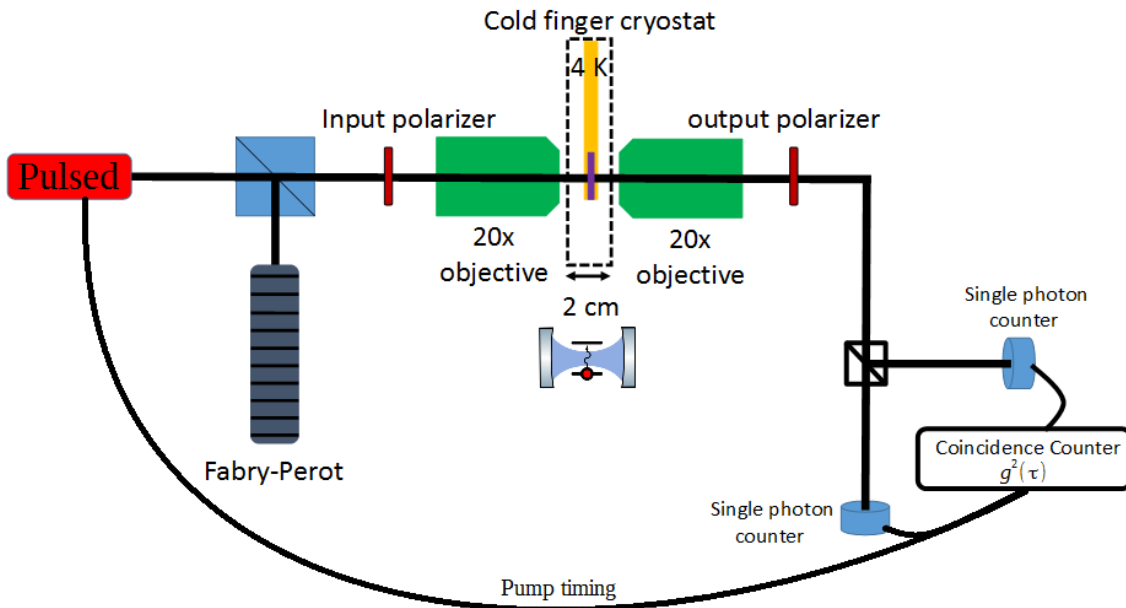


**Figure 5.3:** A schematic overview of the experimental setup with the pulsed laser. The additional cable from the laser to the coincidence counter can be used as a stop signal for the timer.

The setup is mostly identical to before, except that on top of the Hanbury-Brown-Twiss setup we can also use the pump for the pulsed laser as the stop signal for the timer in the coincidence counter. In that configuration we only use one of the two single photon detectors, and this can be used to measure the time-dependent response of the system to a pulse (instead of the autocorrelation function).

## 5.3 Methods

With this new setup we can perform three types of measurements, all of which are presented in the next section.

- Firstly we can use the Hanbury-Brown-Twiss setup to detect the autocorrelation function of the light emitted by the quantum dot when pumped by a pulsed laser. The expected

shape of this autocorrelation function differs significantly from that of a QD pumped by a continuous wave laser, as we will discuss below.

- Secondly we will use this setup to look for Rabi oscillations. This is done by recording the single count rate of the photodetectors over a wide range of input laser power.
- Thirdly we can use the timing of the pulsed laser (with a repetition rate of 80 MHz, i.e. a single pulse every 12.5 ns) as the stop signal for the timed measurement, which will give us a histogram of the emitted single photons as a function of time after the pulse is received.

One side remark that needs to be made is that we have chosen to perform all these measurements in the ‘90Cross’ configuration. We have previously established that the ‘45Circ’ or ‘Optimal’ configuration will lead to higher brightness without a loss in purity. However we have seen experimentally that the outgoing light is of sufficient intensity to perform accurate and quick measurements even in the ‘90Cross’ configuration.

Furthermore the completely flat lineshape of this configuration in the absence of a quantum dot allows for accurate calibration of the optical elements in the beam path. Since the purity of the quantum dot is very sensitive to the alignment of these elements the ‘90Cross’ configuration is therefore the most ideal configuration to work with, provided the intensity is high enough for good measurements.

Thirdly since the laser pulses are very narrow in time, 50 ps, they are relatively broad written in the frequency domain. This means that the non-zero background close to the QD resonance frequency in the ‘45Circ’ and ‘Optimal’ configuration (see figure 4.2) will transmit too much laser light to perform good SPS measurements.

### 5.3.1 $g^2(\tau)$ of a pumped system

We have before investigated the expected shape of the autocorrelation function  $g^2(\tau)$  of a single photon source pumped by a continuous wave laser. Furthermore we investigated the influence of impurity on the dip in this autocorrelation function, and calculated how to extract the SPS purity from the experimental results. In this section we will take a closer look at the expected  $g^2(\tau)$ -curve for a quantum dot pumped with a pulsed laser, and comment on the applicability of the earlier analysis on purity in this setting.

A pulsed laser sends tightly bunched packets of photons at regular intervals. The autocorrelation function of such a system looks like very sharp peaks spaced apart at exactly the repetition rate (time between concurrent packets of photons). When this is used to excite a QD the resulting emission consist of single photons, spaced apart by the repetition rate. This means that the autocorrelation function of the emitted single photons will also show sharp peaks at (multiples of) the repetition rate of the pump laser. However, the autocorrelation at 0 time delay,  $g^2(0)$ , will still in theory be exactly 0 as there is no chance of detecting two photons at the same time. This means that in theory the height of any observed signal at  $\tau = 0$  is a measure for the purity of the quantum dot.

Furthermore, the count bleeding in the  $g^2(\tau)$ -measurement due to the detector response func-

tion is reduced in measurements of the pulsed autocorrelation function since there are (almost) no coincidence counts not just at  $\tau = 0$  but also almost no counts for  $\tau$  close to zero. More specifically: as long as the detector jitter is well below the repetition rate of the pulsed laser, it is irrelevant and the purity measurements are perfectly accurate. This means that we can get much better purity measurements in the pulsed configuration.

There are two assumptions in the analysis on  $g^2(\tau)$  of a mixed beam that might not hold for a system driven by a pulsed laser, each of which might invalidate the conclusion. However, we claim that the final result still holds. Below we discuss these two points.

Firstly we have neglected an interference term in the derivation of our final result in chapter 3, which was allowed in the continuous wave setting since the quantum dot samples randomly from all the phases of the applied laser light. In the pulsed setting the exact reverse happens: the pulse duration is significantly shorter than the decay time of the quantum dot (50 ps versus 2.7 ns, see figures 5.6 and 5.7). Since a pulse with a well-defined energy has a definite number of photons it has no global phase, so averaging over the entire pulse means that still there is no correlation between photon phase and QD excitation.

Secondly we used the fact that our cavity is in equilibrium to justify using a coherent state to describe the laser light. Since the applied laser light is explicitly time-dependent in the pulsed setting this motivation no longer holds. However the wave packets emitted by the laser are still best described as coherent states (with a time dependent amplitude), meaning that this model is still appropriate for the pulsed setting.

We conclude that, similar to before, the purity of the SPS can be determined from the height of the autocorrelation function at  $\tau = 0$ .

## 5.4 Measurements

In this section we present the experimental results acquired with the methods explained above. We will first present the autocorrelation function results, secondly the data on Rabi oscillations, and thirdly the measured decay rate of the quantum dot.

### 5.4.1 $g^2(\tau)$ of a pulsed quantum dot

Figure 5.4 presents the measured  $g^2(\tau)$ -function of the QD in the pulsed setup.

We see that almost no peak is visible at zero time delay, whereas the expected peaks at multiples of the repetition rate 12.5 ns are clearly visible. Comparing the peak heights shows that the peak around  $\tau = 0$  is approximately 6% of the height of the neighbouring peaks, putting the pulsed SPS at 97% purity. However due to the detector response broadening all measured data it is more accurate to compare the area of the central peak with the neighbouring ones

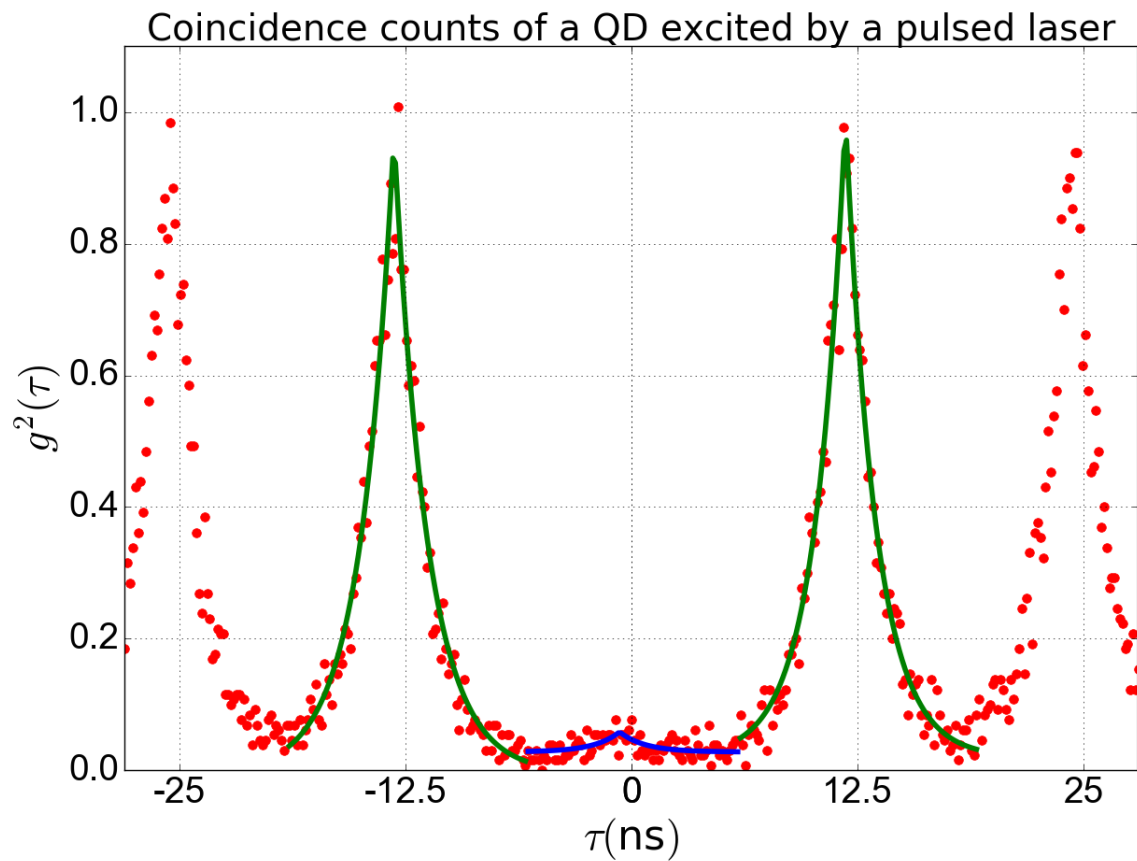


**Figure 5.4:** Experimentally observed autocorrelation function of a quantum dot excited by a pulsed laser with a repetition rate of 12.5 ns. The lines are double exponentials fit to the data.

[8]. Using this method to compute the purity gives us 98%, confirming that our system acts as a good SPS.

### 5.4.2 Rabi oscillation measurements

Figure 5.5 presents our measured single count rate on the detector (corresponding to the intensity of the emitted light) as a function of the applied laser power. The power is measured before the cavity, the discussion on converting this scale to the power inside the cavity can be found below.

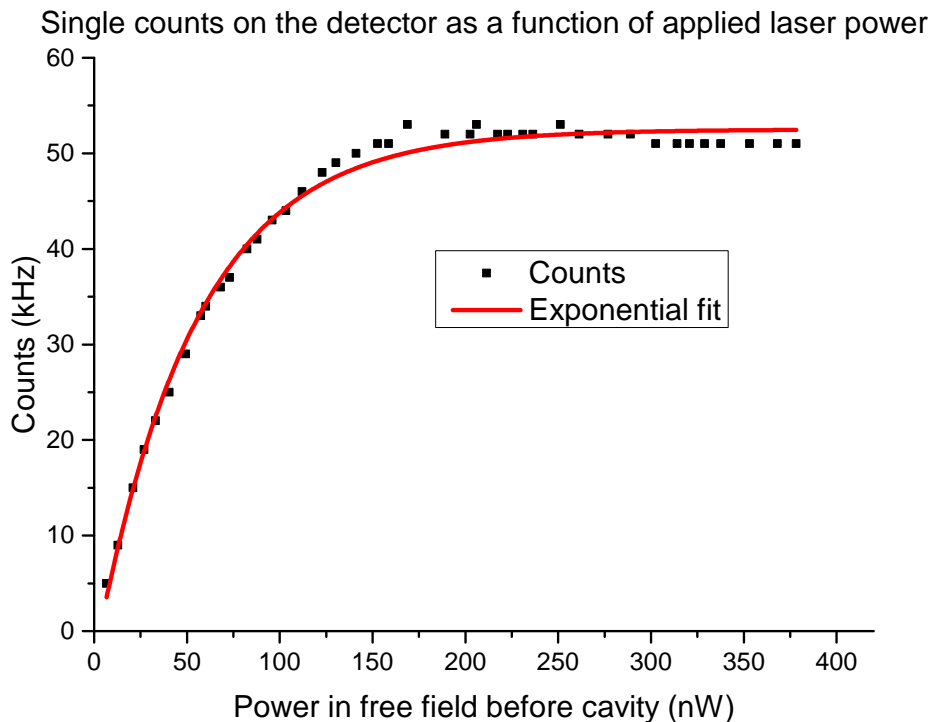


**Figure 5.5:** The single counts on the detector, corresponding to the intensity of the light emitted by the quantum dot, versus the applied laser power. An exponential fit corresponding to a saturation curve was included for comparison.

The good agreement between the observed data and the simple exponential curve indicate that there are no signs of a Rabi oscillation at all. The slight decrease in counts at the high power end of the measurement, as well as the slightly higher count rate around 170 nW, is most likely due to slight cavity drift (physically drifting out of the center of the beam path) during the measurement. During this measurement the data points at 250 nW, 205 nW and 170 nW were measured near the start of the experiment, and the rest later, so their deviation is consistent with cavity drift. Below we will first explain why our range of laser power is the right energy scale for observing Rabi oscillations, and then discuss potential causes that might prevent these oscillations from being present in our system.

We need to convert the horizontal axis to energy per pulse, i.e. number of photons in each pulse, inside the cavity. The power is measured in a free space part of the setup outside the cavity. From there the coupling to the cavity mode is 0.5%, so the 400 nW power corresponds to 2 nW at the cavity mode. However, to ensure that most of the light created by the quan-

tum dot is sent to the detectors we need to tune the quantum dot emission frequency to the outgoing polarization mode, which means that it is placed in the tail of the lineshape of the input polarization mode (since the cavity is polarization non-degenerate these two frequencies differ). This means that we lose another factor of approximately 5 in the coupling. We therefore expect the average power in the input cavity mode to be 0.4 nW at the highest power used in the measurement. Since the repetition rate of the pulsed laser is 80 MHz this corresponds to  $5 \times 10^{-18}$  J per pulse, or roughly 22-23 photons per pulse.

To extract the number of Rabi oscillations that we expect from these 22-23 photons per pulse in the input polarization mode we need to consider one more coupling strength: the influence of the quantum dot angle. In our experiment the QD angle was determined to be  $\theta_{\text{QD}} = 94^\circ$ , which gives an intensity coupling strength of  $\cos^2(\theta_{\text{QD}}) \approx 0.005$ . Since the cooperativity of the QD is  $C = 1$  this means that our 22-23 photons correspond to a  $0.1\pi$ -pulse, far less than a single Rabi oscillation. However, the experimental data clearly disagrees with this number – the QD is saturated around 150 nW input power, so even half the maximum power is already enough to elevate the QD to the excited state with nearly every pulse! We expect that this disagreement between theory and experiment is due to the QD angle. We have seen before in the continuous wave measurements that the ‘90Cross’ configuration leads to higher transmission than expected, and proposed that the cause of this is the local electronic configuration influencing the dipole of the quantum dot. This mechanism could change the QD angle at the specific applied voltage we are measuring at. From the extraordinary transmission in the continuous wave experiment, which was 10 times the expected intensity, we can deduce that the QD angle for this voltage is  $103^\circ$  instead of  $94^\circ$ , increasing the value of  $\cos^2(\theta_{\text{QD}})$  to 0.05. This would imply that at the highest power we applied a  $\pi$ -pulse with every pulse of the laser. However, the power for a Rabi  $\pi$ -pulse is necessarily lower than the saturation constant in the exponential fit of the measured count rate, since coherent excitation is the most efficient mechanism to bring the quantum dot to the excited state. This means that the above analysis underestimates the coupling efficiency of the measured power to the QD by at least a factor 2. In particular the value of the cooperativity and the on-resonance coupling of the applied field to the cavity polarization mode might be a factor 2 higher than previously estimated. All in all we conclude that the power range investigated in the experiment corresponds to the order of a Rabi oscillation, so it is surprising that none are visible in the data.

There are a few potential explanations for the absence of Rabi oscillations in the experimental data.

Firstly the amplitude of Rabi oscillations decreases exponentially with the oscillation number (the first oscillation is exponentially larger than the second one, which is exponentially larger than the third oscillation, etc.). It might therefore be of interest to take a closer look at the lower power ranges, from 0 nW to 50 nW on the experimental schale in figure 5.5. However due to the good fit of the exponential saturation we believe that the absence of Rabi oscillations in this data is not just an artefact of sampling, but has a physical cause.

Secondly the absence of Rabi oscillations might naively be attributed to the presence of other quantum dots in the system, whose oscillations could interfere destructively. However the autocorrelation measurements show that the transmitted light consists of at least 98% single photons, which means that this interference could be at most 2% of the signal. This explana-

tion is therefore not sufficient to explain the lack of oscillations.

Thirdly simulations show that in this QD-cavity setup Rabi oscillations are sensitive to a number of non-linear effects such as phonon interaction and multi-photon absorption. This makes these oscillations challenging to observe, which potentially contributes to the absence of visible oscillations.

All in all it is at the moment of writing this not clear why no Rabi oscillations were found in this experiment.

### 5.4.3 Decay rate

By using using the 80 MHz signal of the pulsed laser as the start signal in the detection setup we can observe the time-dependent emission of the QD excited by the pulsed laser.

Figure 5.6 shows the measured time-tagged counts on a logarithmic scale for three different measurements: two at different laser power (with 3 KHz single counts on the detector and 1.8 KHz single counts on the detector respectively) and one with the voltage over the cavity set to such a value that no quantum dot was excited by the pulsed laser light. Figure 5.7 shows the fitted lifetime of the quantum dot as a function of the applied laser power.

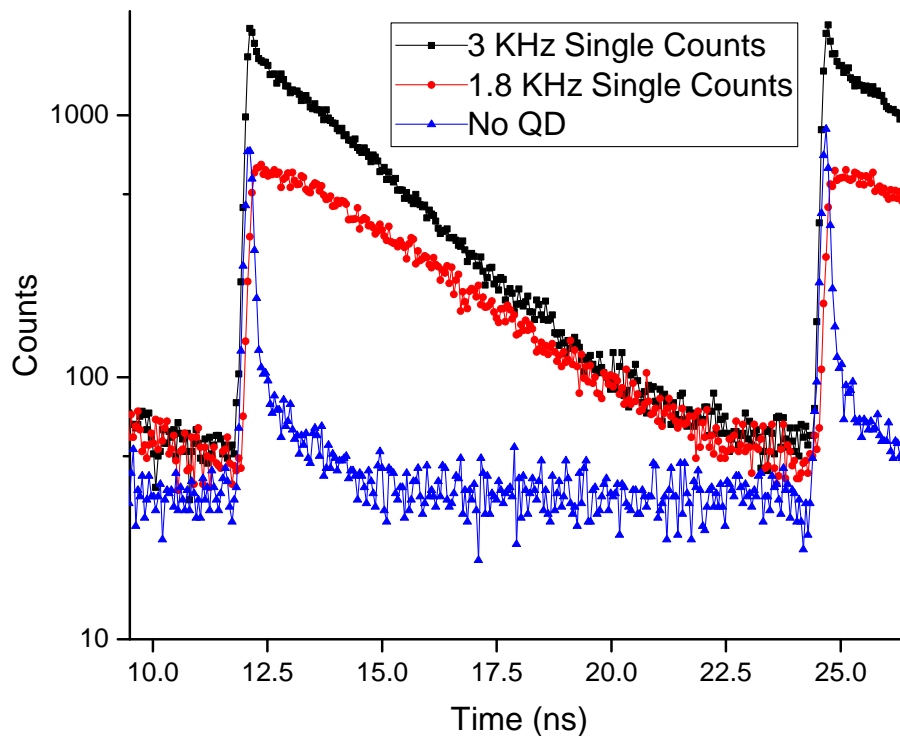


**Figure 5.6:** The number of counts on the photodetector as a function of time after the laser pulse is sent through the system. A delay time of 12.5 ns coincides with exactly the repetition rate of the laser.

First we remark that the ‘No QD’ dataset shows the pulse width of the light passing through the empty is around 300 ps (the FWHM of the pulse is 6 data points, which are spaced approximately 0.05 ns apart). This is in good agreement with the measured detector jitter of 350 ps in figure 4.1.

Next we note that the straight lines (on a logarithmic scale) of the two sets of measurements on the QD indicate that we are observing a simple exponential decay process – the decay rate of the QD in the cavity. But the two different slopes indicate that the decay rate of the quantum dot is sensitive to the applied laser power. In particular the decay time fitted from the ‘3 KHz’ measurement is 2.5 ns, whereas the decay time fitted from the ‘1.8 KHz’ measurement is 3.5 ns, a significant difference. To further study this we measured the decay rate of the QD for a wider range of input laser power, shown below in figure 5.7.

There are several observations that we can make about this dataset. Most importantly these measurements are not consistent with a fixed QD decay rate, which is what we would expect in our setup and is also present in the full quantum master equation simulations of our system. Below we will discuss these measurements.

Firstly we would like to mention that the decay rate in figure 5.6 for the dataset with 1.8KHz

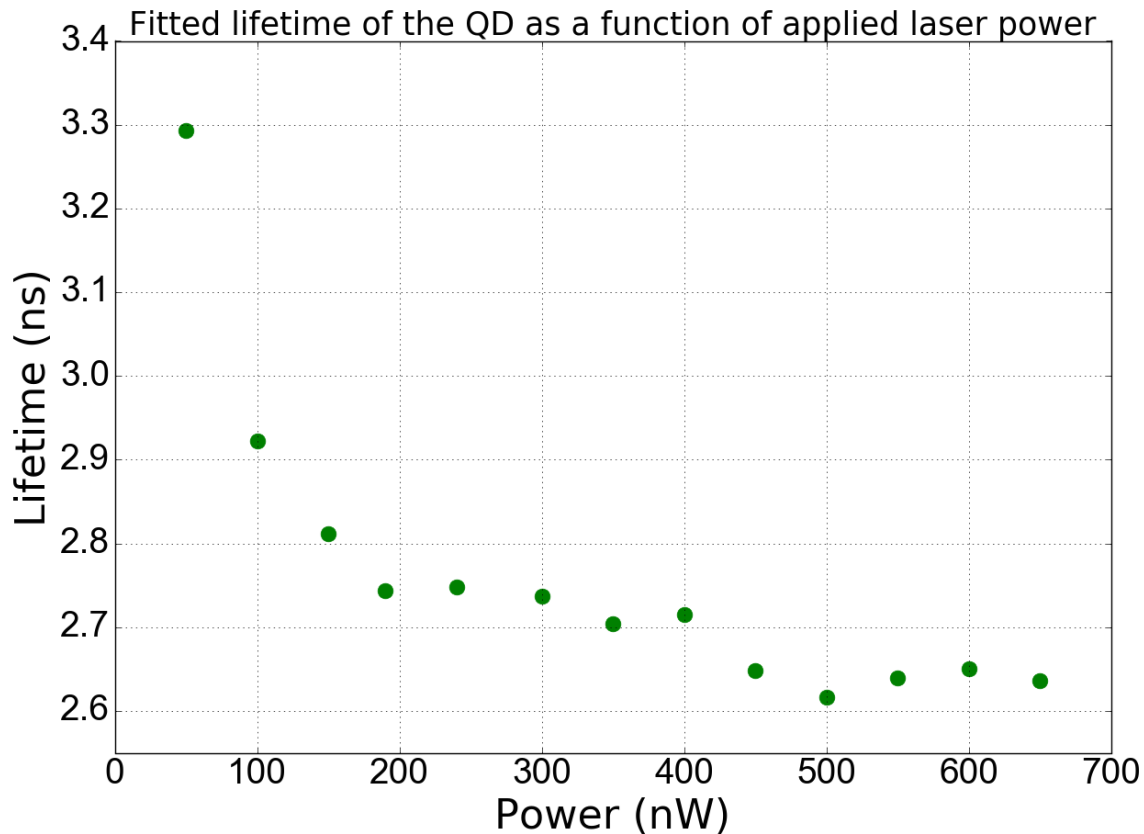


**Figure 5.7:** The measured decay rate of the QD in the cavity as a function of applied laser power.

counts, given as 3.5 ns, is larger than any of the decay rates from the second experiment. The power in the 1.8KHz measurement was 50 nW, the same as the first datapoint from the second measurement set. While we would therefore expect the decay rate to be high, it is not clear what causes it to be this far above all the other measurements.

Secondly we note that this unexpected dependency has been seen before in weakly coupled InAs/GaAs quantum dots in a 1D waveguide [28], where the authors provide a phenomenological theory to predict this behaviour. Furthermore change in the decay rate has been observed in a photoluminescence measurement [29] and in a photoluminescence measurement of colloidal CdSe quantum dots [30], where the authors suggest that non-radiative decay pathways are effected by the applied intensity. However [30] clearly observe multiexponential behaviour in their measurements, whereas all our decay curves (as well as those shown by [28]) are single exponential.

Thirdly we note that in the absence of a quantum dot in the cavity the pulse has left the cavity after 100 ps at the latest (laser pulse width and cavity lifetime) after reaching it. This means that for almost the whole duration of the QD decay, which takes on the order of 3 ns, there is no light present in the cavity. This suggests that the change in the decay rate of the QD is not caused by the dot-cavity interaction but rather by a coupling of the QD excited state to a non-radiative energy mode. The only available mechanism for this is phonon coupling to

the QD. A potential mechanism for how the QD-phonon coupling is dependent on the applied electric field could be the realignment of the QD dipole along the electric field, keeping in mind that the applied field is strong enough that we are in the strong coupling regime. Such a shift of the dipole could also influence the coupling to phonon states. However if this were the case we would expect to see a multi-exponential decay, showing both the lifetime of the QD-phonon interaction and the QD-cavity interaction. In conclusion we cannot say more than that additional research is needed to determine the exact mechanism through which the optical field influences the decay rate.

Finally we remark that the unexpected behaviour of the lifetime of the QD might be related to the absence of Rabi oscillations in our earlier measurements. If the lifetime changes are indeed due to a changing coupling strength to a non-radiative decay mode we would expect the amount of created single photons to also be effected by this, making Rabi oscillations less pronounced.

## Conclusion

We have shown through theory and simulation that in order to use a quantum dot in an optical cavity as a single photon source it is best if the cavity is polarization non-degenerate. Furthermore simulation and experiment have proven that by using non-linear polarization configurations for such a cavity-plus-quantum dot system we can achieve an increased intensity of the single photon source without sacrificing purity.

We proceeded to give two different theoretical derivations of determining the autocorrelation function,  $g^2(\tau)$ , of light created by mixing different sources. The resulting formula can be used to determine the purity of a single photon source from a measurement of the autocorrelation function. By comparing the two derivations we conclude that in the limit of low power a quantum mechanical description of mixing of light and a classical description of mixing of light give the same result for the autocorrelation function.

Lastly we conducted several measurements of the quantum dot excited by a pulsed laser. We observed that the autocorrelation function for this measurement has approximately 4% coincidence counts by area at  $\tau = 0$ , indicating that this setup acts as a single photon source with a high purity of 98%. However, our system exhibits no signs of Rabi oscillations. Furthermore we experimentally detected that the lifetime of the quantum dot is dependent on the power of the pulse sent to the cavity. Further research is needed to investigate these last two phenomena.



# Bibliography

- [1] C. H. Bennett and G. Brassard, *Quantum Cryptography: Public Key Distribution, and Coin-Tossing*, Proc. 1984 IEEE International Conference on Computers, Systems, and Signal Processing , 175 (1984).
- [2] K. Chen, C. M. Li, Q. Zhang, Y. A. Chen, A. Goebel, S. Chen, A. Mair, and J. W. Pan, *Experimental realization of one-way quantum computing with two-photon four-qubit cluster states*, Physical Review Letters **99**, 1 (2007).
- [3] I. Aharonovich, D. Englund, and M. Toth, *Solid-state single-photon emitters*, Nature Photonics **10**, 631 (2016).
- [4] D. Cadeddu, J. Teissier, F. R. Braakman, N. Gregersen, P. Stepanov, J.-M. Gérard, J. Claudon, R. J. Warburton, M. Poggio, and M. Munsch, *A fiber-coupled quantum-dot on a photonic tip*, Applied Physics Letters **108**, 011112 (2016).
- [5] A. Jeantet, Y. Chassagneux, C. Raynaud, P. Roussignol, J. Lauret, B. Besga, J. Estève, J. Reichel, and C. Voisin, *Widely Tunable Single-Photon Source from a Carbon Nanotube in the Purcell Regime*, Physical Review Letters **116**, 247402 (2016).
- [6] J. L. Zhang, S. Sun, M. J. Burek, C. Dory, Y.-K. Tzeng, K. A. Fischer, Y. Kelaita, K. G. Lagoudakis, M. Radulaski, Z.-X. Shen, N. A. Melosh, S. Chu, M. Loncar, and J. Vuckovic, *Strongly Cavity-Enhanced Spontaneous Emission from Silicon-Vacancy Centers in Diamond*, ArXiv:1708.05771 (2017).
- [7] X. He, N. F. Hartmann, X. Ma, Y. Kim, R. Ihly, J. L. Blackburn, W. Gao, J. Kono, Y. Yomogida, A. Hirano, T. Tanaka, H. Kataura, H. Htoon, and S. K. Doorn, *Tunable room-temperature single-photon emission at telecom wavelengths from  $sp^3$  defects in carbon nanotubes*, Nature Photonics (advanced online publications) , 1 (2017).
- [8] H. J. Snijders, J. A. Frey, J. Norman, V. P. Post, A. C. Gossard, J. E. Bowers, M. P. van Exter, W. Löffler, and D. Bouwmeester, *A fiber coupled cavity QED source of identical single photons*, ArXiv:1705.05876 , 1 (2017).
- [9] A. Schlehahn, R. Schmidt, C. Hopfmann, J.-H. Schulze, A. Strittmatter, T. Heindel, L. Gantz, E. R. Schmidgall, D. Gershoni, and S. Reitzenstein, *Generating single photons at gigahertz modulation-speed using electrically controlled quantum dot microlenses*, Applied Physics Letters **108**, 021104 (2016).

- 
- [10] X. Ding, Y. He, Z.-C. Duan, N. Gregersen, M.-C. Chen, S. Unsleber, S. Maier, C. Schneider, M. Kamp, S. Höfling, C.-Y. Lu, and J.-W. Pan, *On-Demand Single Photons with High Extraction Efficiency and Near-Unity Indistinguishability from a Resonantly Driven Quantum Dot in a Micropillar*, Physical Review Letters **116**, 020401 (2016).
- [11] N. Somaschi, V. Giesz, L. De Santis, J. C. Loredo, M. P. Almeida, G. Hornecker, S. L. Portalupi, T. Grange, C. Antón, J. Demory, C. Gómez, I. Sagnes, N. D. Lanzillotti-Kimura, A. Lemaître, A. Auffèves, A. G. White, L. Lanco, and P. Senellart, *Near-optimal single-photon sources in the solid state*, Nature Photonics **10**, 340 (2016).
- [12] M. J. Holmes, S. Kako, K. Choi, M. Arita, and Y. Arakawa, *Single Photons from a Hot Solid-State Emitter at 350 K*, ACS Photonics **3**, 543 (2016).
- [13] K. Müller, K. A. Fischer, C. Dory, T. Sarmiento, K. G. Lagoudakis, A. Rundquist, Y. A. Kelaita, and J. Vučković, *Self-homodyne-enabled generation of indistinguishable photons*, Optica **3**, 931 (2016).
- [14] X.-L. Chu, S. Götzinger, and V. Sandoghdar, *A single molecule as a high-fidelity photon gun for producing intensity-squeezed light*, Nature Photonics **11**, 58 (2016).
- [15] Y.-M. He, J. Liu, S. Maier, M. Emmerling, S. Gerhardt, M. Davanço, K. Srinivasan, C. Schneider, and S. Höfling, *Deterministic implementation of a bright, on-demand single-photon source with near-unity indistinguishability via quantum dot imaging*, Optica **4**, 802 (2017).
- [16] S. Gerhardt, J. Iles-Smith, D. P. S. McCutcheon, Y.-M. He, S. Unsleber, N. Gregersen, J. Mørk, S. Höfling, and C. Schneider, *Intrinsic and environmental effects on the interference properties of a high-performance quantum dot single photon source*, ArXiv:1707.02886 (2017).
- [17] F. Liu, A. J. Brash, J. O 'hara, L. M. P. P. Martins, C. L. Phillips, R. J. Coles, B. Royall, E. Clarke, C. Bentham, N. Prtljaga, I. E. Itskevich, L. R. Wilson, M. S. Skolnick, and A. M. Fox, *High Purcell factor generation of coherent on-chip single photons*, ArXiv:1706.04422 (2017).
- [18] A. Schlehahn, S. Fischbach, R. Schmidt, A. Kaganskiy, A. Strittmatter, S. Rodt, T. Heindel, and S. Reitzenstein, *A stand-alone fiber-coupled single-photon source*, ArXiv:1703.10536 (2017).
- [19] M. P. Bakker, A. V. Barve, A. Zhan, L. A. Coldren, M. P. van Exter, and D. Bouwmeester, *Polarization degenerate micropillars fabricated by designing elliptical oxide apertures*, Applied Physics Letters **104**, 151109 (2014).
- [20] E. Waks and J. Vuckovic, *Dipole Induced Transparency in Drop-Filter Cavity-Waveguide Systems*, Physical Review Letters **96**, 153601 (2006).
- [21] A. Auffèves-Garnier, C. Simon, J.-M. Gérard, and J.-P. Poizat, *Giant optical nonlinearity induced by a single two-level system interacting with a cavity in the Purcell regime*, Physical Review A **75**, 053823 (2007).
-

- 
- [22] M. Bakker, *Cavity quantum electrodynamics with quantum dots in microcavities*, PhD Thesis (2015).
- [23] M. F. van de Stolpe, *Optimizing the polarization for a brighter CQED Single Photon Source*, Master's Thesis (2017).
- [24] V. Giesz, N. Somaschi, G. Hornecker, T. Grange, B. Reznichenko, L. De Santis, J. Demory, C. Gomez, I. Sagnes, A. Lemaître, O. Krebs, N. D. Lanzillotti-Kimura, L. Lanco, A. Auffeves, and P. Senellart, *Coherent manipulation of a solid-state artificial atom with few photons*, Nature Communications **7**, 11986 (2016).
- [25] E. B. Flagg, A. Muller, J. W. Robertson, S. Founta, D. G. Deppe, M. Xiao, W. Ma, G. J. Salamo, and C. K. Shih, *Resonantly driven coherent oscillations in a solid-state quantum emitter*, Nature Physics **5**, 203 (2009).
- [26] R. Bose, T. Cai, K. R. Choudhury, G. S. Solomon, and E. Waks, *All-optical coherent control of vacuum Rabi oscillations*, Nature Photonics **8**, 858 (2014).
- [27] M. P. Bakker, T. Ruytenberg, W. Löffler, A. Barve, L. Coldren, M. P. van Exter, and D. Bouwmeester, *Quantum dot nonlinearity through cavity-enhanced feedback with a charge memory*, Physical Review B **91**, 241305 (2015).
- [28] L. Monniello, C. Tonin, R. Hostein, A. Lemaitre, A. Martinez, V. Voliotis, and R. Grousson, *Excitation-Induced Dephasing in a Resonantly Driven InAs / GaAs Quantum Dot*, Physical Review Letters **111**, 026403 (2013).
- [29] B. R. Fisher, H.-J. Eisler, N. E. Stott, and M. G. Bawendi, *Emission Intensity Dependence and Single-Exponential Behavior In Single Colloidal Quantum Dot Fluorescence Lifetimes*, The Journal of Physical Chemistry B **108**, 143 (2003).
- [30] G. Ramon, U. Mizrahi, N. Akopian, S. Braitbart, D. Gershoni, T. Reinecke, B. Gerardot, and P. Petroff, *Emission characteristics of quantum dots in planar microcavities*, Physical Review B **73**, 205330 (2006).